FRACTALS IN THE TWIST-AND-FLIP CIRCUIT

by

Leon O. Chua, Ray Brown, and Nathan Hamilton

Memorandum No. UCB/ERL M92/77

14 April 1992

COVER PAGE

FRACTALS IN THE TWIST-AND-FLIP CIRCUIT

by

Leon O. Chua, Ray Brown, and Nathan Hamilton

Memorandum No. UCB/ERL M92/77

14 April 1992

ELECTRONICS RESEARCH LABORATORY

College of Engineering
University of California, Berkeley
94720

FRACTALS IN THE TWIST-AND-FLIP CIRCUIT

by

Leon O. Chua, Ray Brown, and Nathan Hamilton

Memorandum No. UCB/ERL M92/77

14 April 1992

ELECTRONICS RESEARCH LABORATORY

College of Engineering
University of California, Berkeley
94720

Fractals in the Twist-and-Flip Circuit

Leon O. Chua, Ray Brown, and Nathan Hamilton

Department of Electrical Engineering and Computer Sciences
University of California, Berkeley

April 14, 1992

Abstract

The twist-and-flip circuit contains only three circuit elements: two linear capacitors connected across the ports of a gyrator characterized by a nonlinear gyration conductance function $g(v_1, v_2)$. When driven by a square-wave voltage source of amplitude "a" and frequency "ω", the resulting circuit is described by a system of two non-autonomous state equations. For almost any choice of nonlinear $g(v_1, v_2) > 0$, and over a very wide region of the $a - \omega$ parameter plane, the twist-and-flip circuit is imbued with the full repertoire of complicated chaotic dynamics typical of those predicted by the classic KAM theorem from Hamiltonian dynamics, and widely observed numerically from plasma and accelerator dynamics, as well as from celestial mechanics.

The significance of the twist-and-flip circuit is that its associated non-autonomous state equations have an explicit Poincaré map, called the twist-and-flip map, thereby making it possible to analyze and understand the intricate dynamics of the system, including its many fractal manifestations.

Although the properties of the twist-and-flip circuit are best understood from an in-depth analysis of its many elegant mathematical properties (published elsewhere), this paper will focus on the many fractals associated with the twist-and-flip circuit, in keeping with the theme of this special issue. Behind the masks of the colorful fractals, however, lies an immensely rich variety of chaotic phenomena, whose unique mathematical tractability is responsible for this circuit's potential application as a paradigm for "non-autonomous" chaos.

This work is supported in part by the Office of Naval Research under grant N00014-89-J-1402 and the National Science Foundation under grant MIP-8912639

1 Introduction

Chaos is a robust nonlinear phenomenon that permeates all fields of science and technology, and fractals are but one of its many manifestations. Nowhere is this phenomenon more easily demonstrated, analyzed, and synthesized than in simple autonomous nonlinear electronic circuits; namely, circuits without ac sources and therefore described by an autonomous system

$$\dot{\mathbf{x}} = f(\mathbf{x}) \tag{1}$$

of ordinary differential equations, where $\mathbf{x}$ is a vector in an n-dimensional Euclidean space $\mathbf{R}^n$. For example, the simplest paradigm of "autonomous" chaos is given by Chua's circuit [1-3], which contains only one linear resistor, one linear inductor, two linear capacitors, and a two-terminal nonlinear resistor called the Chua diode [4]. Because of its mathematical tractability, more than 50 in-depth analyses of Chua's circuit have been published on all aspects of this circuit, including the fractal nature of its many bifurcation diagrams.

But chaos can also occur in non-autonomous systems; namely, systems driven by time-varying (ac) signals, and therefore described by a non-autonomous system of ordinary differential equations

$$\dot{\mathbf{x}} = f(\mathbf{x}, t) \tag{2}$$

Our goal in this paper is to present a new non-autonomous electronic circuit, henceforth called the twist-and-flip circuit, which is unique in the sense that it has an explicit mathematical solution. In particular, numerous fractals associated with this circuit can be painlessly generated via the associated Poincaré map, called the twist-and-flip map, which surprisingly, can be expressed in explicit analytic form. Since the state equations associated with the twist-and-flip circuit are the only known non-autonomous system of ordinary differential equations whose Poincaré map can be derived in explicit analytic form, thereby making it possible to carry out an exhaustive and rigorous mathematical analysis, we believe that the twist-and-flip circuit will become the standard paradigm for "non-autonomous" chaos in second-order chaotic systems.

An in-depth mathematical analysis of the twist-and-flip map can be found in [5,6]. In this paper, we will focus our discussion on the various fractals

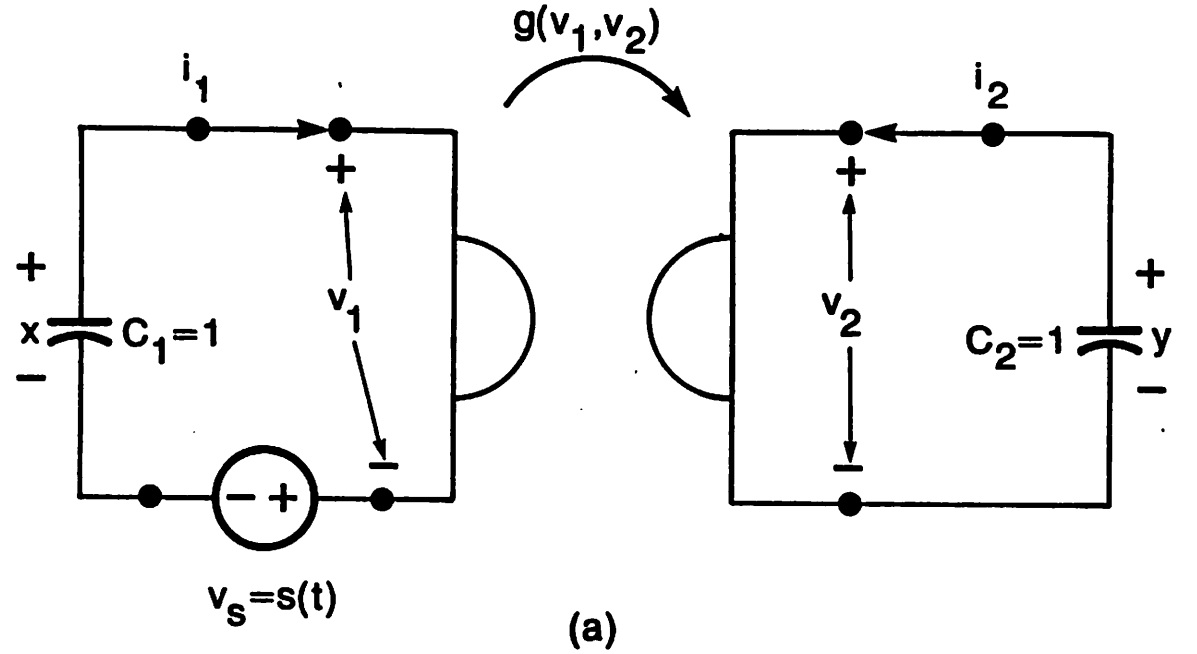

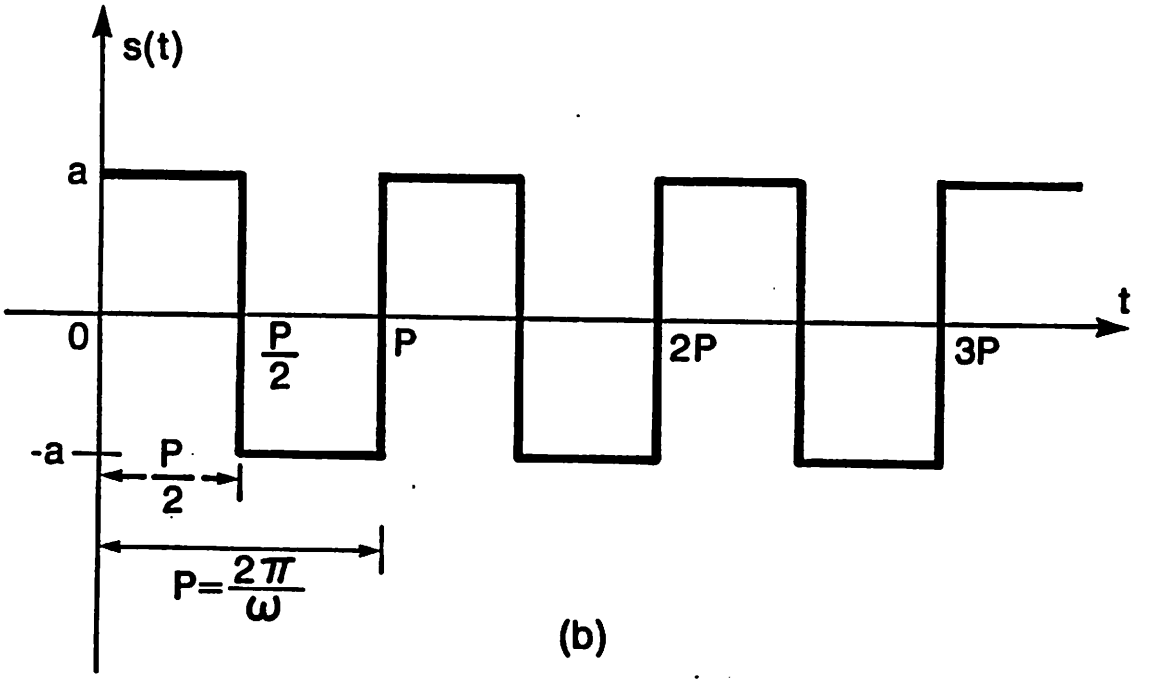

Fig. 1

generated from this map. In addition to presenting a gallery of fractals corresponding to several classes of nonlinear gyration conductance functions $g(v_1, v_2)$, an analysis and interpretation of these fractals, especially in the context of well-known geometric structures (e.g., hyperbolic and elliptic regions, island chains, homoclinic tangles, as well as the evolution and breakup of cantori's etc.) associated with the KAM theorem will be given. The fact that the twist-and-flip map is endowed with the same structures is extremely significant because no other nonlinear conservative system is known to posses an explicit Poincaré map. Even the widely-cited standard map [7] is only a model for mimicking the actual Poincaré map of some classes of Hamiltonian systems. In other words, the standard map is not the Poincaré map of any known non-autonomous system of ordinary differential equations. In contrast, the explicit twist-and-flip map is the exact Poincaré map of the twist-and-flip circuit.

Finally, we will present a series of numerical examples, which shows that in the limit where the gyration conductance function tends to a "Signum function", the invariant manifolds tend to a fractal. We believe this new discovery is highly significant because it represents the first direct link between the dynamics of the trajectories and the associated fractals.

2 The Twist-and-Flip Circuit

Consider the circuit shown in Fig. 1 henceforth called the twist-and-flip circuit.

FIGURE 1

It contains two linear capacitors, C_1 and C_2, which for simplicity, are normalized to one Farad each, a voltage source $V_s = s(t)$, where $s(t)$ denotes a square wave (Fig. 1(b)) of amplitude a and angular frequency ω (or period $P = 2\pi/\omega$), and a gyrator described by

$$i_1 = g(v_1, v_2)v_2 \quad (3a)$$
$$i_2 = -g(v_1, v_2)v_1 \quad (3b)$$

where $g(v_1, v_2)$ is the associated gyration conductance [8]. Note that unlike the original definition where $g(v_1, v_2) = G$ is a constant, this parameter is a

nonlinear function of the port voltages v_1, and v_2 in the twist-and-flip circuit, and henceforth will be referred to as the gyration conductance function. Although a gyrator can be defined by any nonlinear function $g(v_1, v_2)$ in this paper, we will assume that

$$g(v_1, v_2) > 0, \quad \text{for} \quad -\infty < v_1, v_2 < \infty$$

2.1 State equations of the twist-and-flip circuit

Applying KCL, KVL, and the constitutive relation for the capacitors, we obtain

$$i_1 = -C_1 \frac{dx}{dt} = -\frac{dx}{dt} \qquad i_2 = -C_2 \frac{dy}{dt} = -\frac{dy}{dt}$$

$$v_1(t) = x(t) - s(t) \qquad v_2(t) = y(t)$$

It follows from the above equations and the constitutive relation (Eq.4) of the gyrator that the dynamics of the twist-and-flip circuit are governed by the following state equations:

$$\frac{dx}{dt} = -g(x - s(t), y)\, y \qquad (5a)$$

$$\frac{dy}{dt} = g(x - s(t), y)\,(x - s(t)) \qquad (5b)$$

where,

$$s(t) = a, \quad t \in (n, n + 1/2)P \quad \text{(positive half cycle)}$$

$$s(t) = -a, \quad t \in (n + 1/2, n + 1)P \quad \text{(negative half cycle)}$$

$n = 0, 1, 2, ...,$ We can divide Eq.(5b) by (5a) to obtain

$$\frac{dy}{dx} = -(x - a)/y \qquad (6a)$$

over each positive half cycle, and

$$\frac{dy}{dx} = -(x + a)/y \qquad (6b)$$

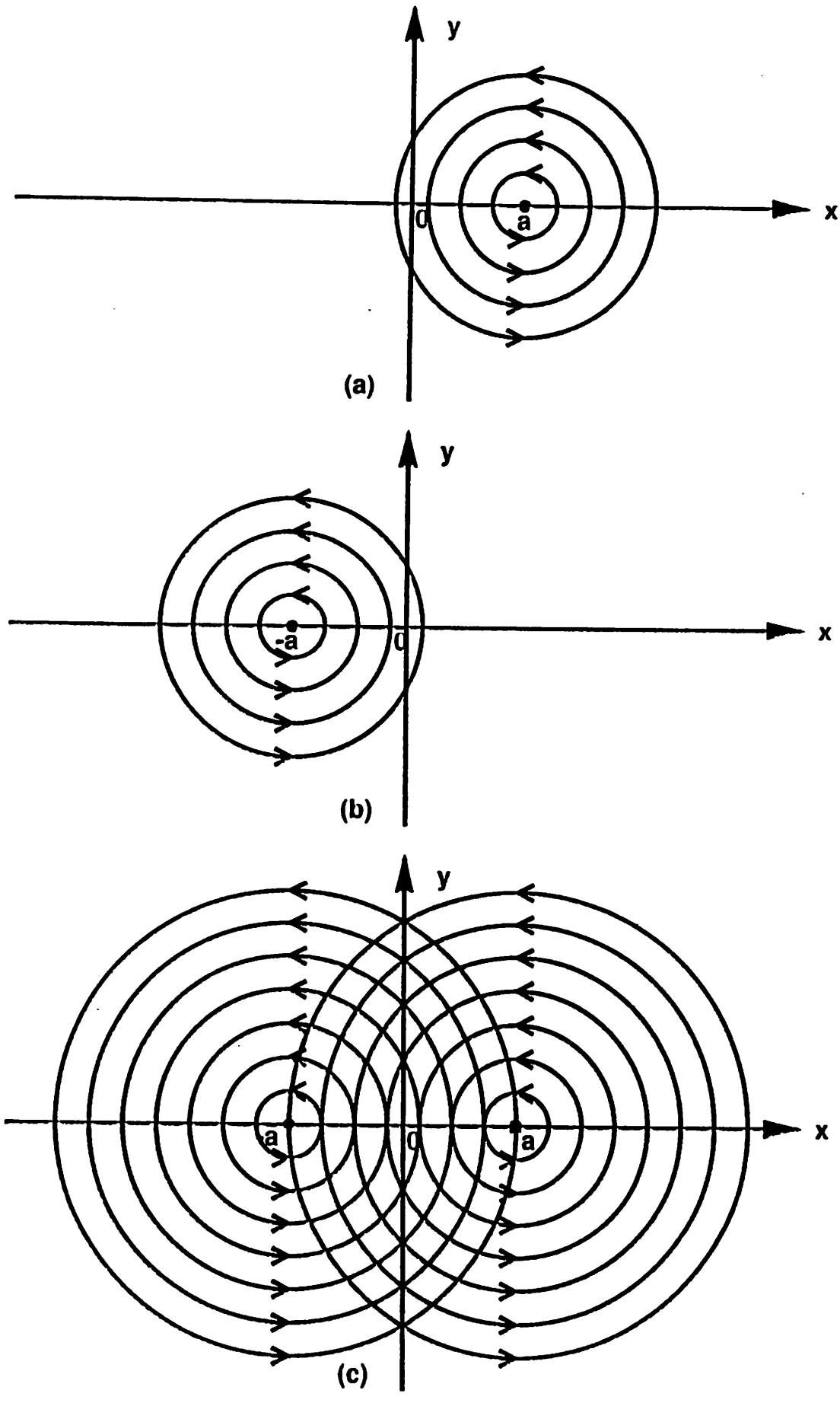

Figure 2

FIGURE 2

over each negative half cycle. Equation (6) defines a phase portrait [9] consisting of a family of concentric circles, centered at $x = a$ (Fig. 2(a)) over each positive half cycle $t \in (n, n + 1/2)P$, and at $x = -a$ (Fig. 2(b)) over each negative half cycle $t \in (n + 1/2, n + 1)P$, $n = 0, 1, 2, ...$ Observe that all trajectories traverse around the circles in a counterclockwise direction because Eqs. (4) and (5a) imply that in the upper half plane where $y > 0$ (resp., lower half plane where $y < 0$),

$$\frac{dx(t)}{dt} < 0$$

resp.,

$$\frac{dx(t)}{dt} > 0$$

Observe also from Eq.(5a) that the time it takes a trajectory to traverse from any point (x_a, y_a) to another point (x_b, y_b) on a circle of radius

$$r_0 = \sqrt{(x_0 \mp a)^2 + y_0^2} \qquad (7)$$

where the upper sign (resp. lower sign) henceforth pertains to the circles centered at $x = a$ (resp, $x = -a$), is given by

$$\begin{aligned} t_{ab} &= t_b - t_a \\ &= \int_{x_a}^{x_b} \frac{-1}{g(x \mp a, y)y} dx \end{aligned} \qquad (8)$$

where y in Eq (8) is replaced by

$$y = \sqrt{r_0^2 - (x \mp a)^2} \qquad (9)$$

before performing the integration

2.2 Explicit solution of the twist-and-flip circuit

In general, Eq. (8) can not be integrated explicitly for arbitrary $g(v_1, v_2)$. However, in this paper, we will henceforth assume that

$$g(v_1, v_2) = f(\sqrt{v_1^2 + v_2^2}) \qquad (10)$$

where $f(\cdot)$ is a single-valued function of only one variable $r = \sqrt{v_1^2 + v_2^2}$.

Under this standing assumption,

$$g(x \mp a, y) = f(r_0) \qquad (11)$$

is a constant since r_0 is fixed by the initial condition (x_0, y_0) via Eq. (7). In this case, Eq. (8) can be integrated explicitly as follows:

$$\begin{aligned} t_{ab} &= t_b - t_a \\ &= \frac{-1}{f(r_0)} \int_{x_a}^{x_b} \frac{dx}{\sqrt{r_0^2 - (x \mp a)^2}} \\ &= \frac{-1}{f(r_0)} [\arcsin((x_b \mp a)/r_0) - \arcsin((x_a \mp a)/r_0)) \\ &= \frac{\theta_b - \theta_a}{f(r_0)} \qquad (12) \end{aligned}$$

where θ_a denotes the angle (in radians) measured from the right of the horizontal axis centered at $x = \pm a$ to (x_a, y_a), and θ_b denotes the corresponding angle measured from $x = \pm a$ to (x_b, y_b). It follows from Eq. (12) that the period P for a trajectory to traverse a circle of radians r once is given by

$$P = \frac{2\pi}{f(r)} = \frac{2\pi}{\omega} \qquad (13)$$

where $\omega = f(r)$. Observe that just as in the familiar harmonic oscillator, the period is equal to $2\pi/\omega$. There is a crucial difference here, however, in that the angular frequency ω in the twist-and-flip circuit is not a constant, but is rather determined by the gyration conductance function $f(r)$. We will see in Section 4 that different choices of $f(r)$ give rise to drastically different dynamics. Since the trajectories associated with the state equations (5) over

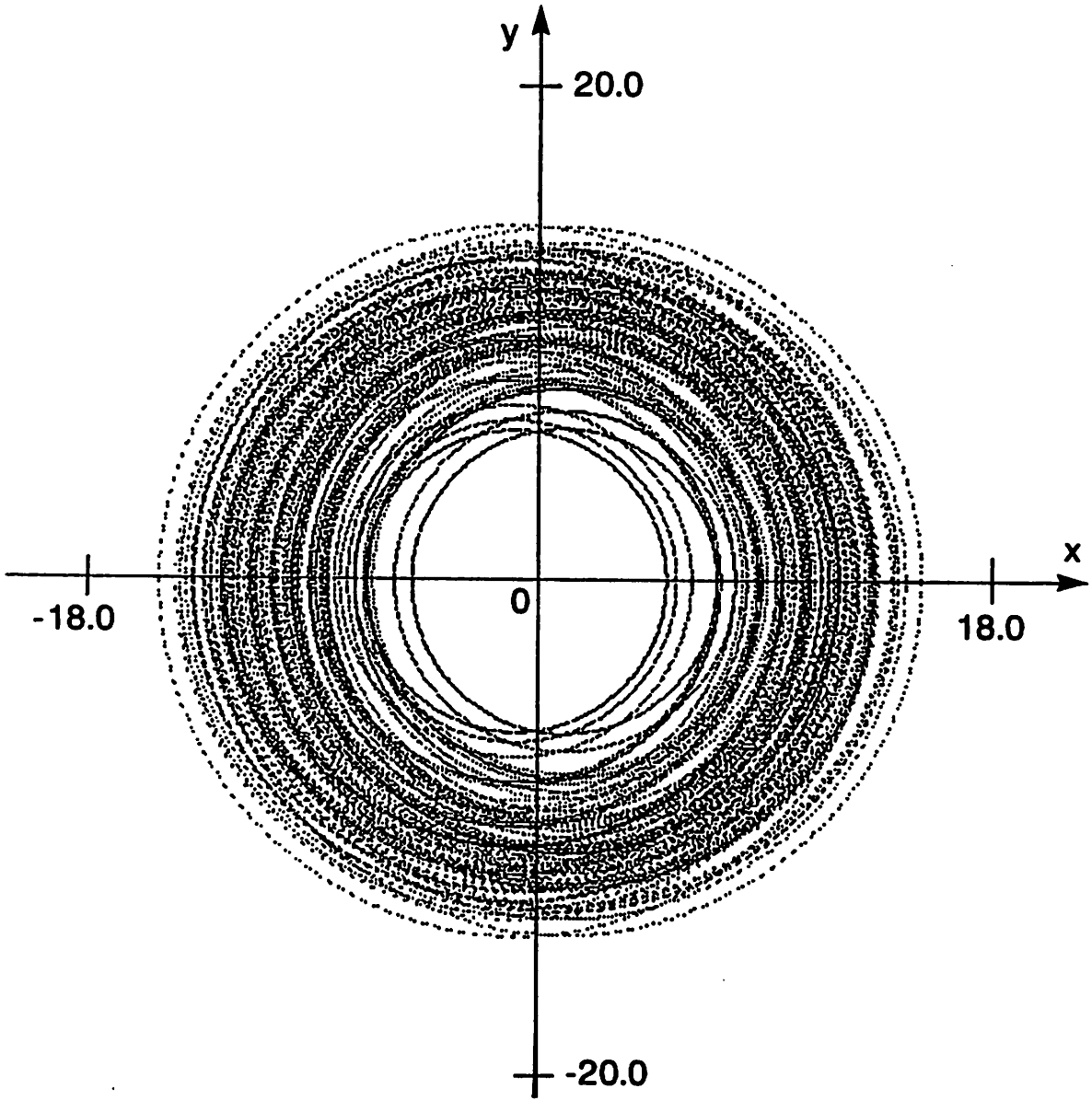

Fig. 3(a)

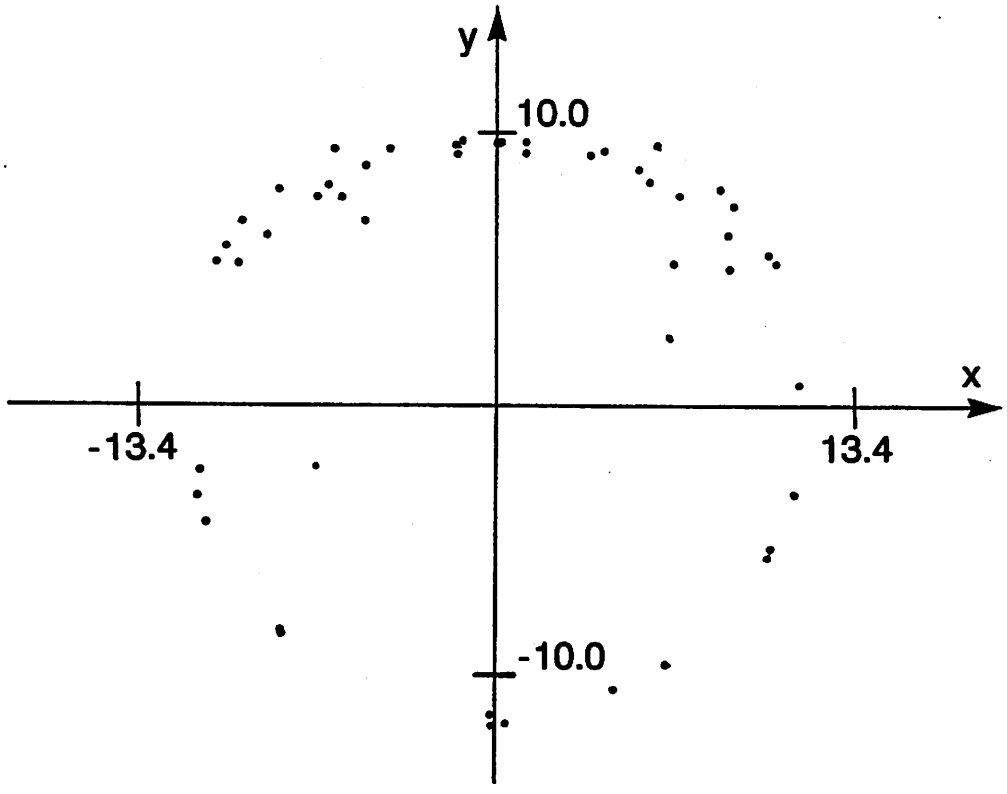

Fig. 3(b)

each half period must fall on circles, as shown in Fig. 2(c), it follows from Eq.(11) that given any initial condition (x_0, y_0), Eq.(5) is equivalent to

$$\frac{dx}{dt} = -f(r_0)y \qquad (14a)$$

$$\frac{dy}{dt} = f(r_0)(x \mp a) \qquad (14b)$$

where the upper sign (resp., lower sign) in Eq. (14b) applies to each positive (resp. negative) half cycle of the square wave input signal $s(t)$.

The solution of the twist-and-flip circuit in Fig. 1 is therefore given explicitly by:

$$x(t) = (x_0 \mp a)\cos(f(r_0)t) - y_0 \sin(f(r_0)t) + a \qquad (15a)$$

$$y(t) = (x_0 \mp a)\sin(f(r_0)t) + y_0 \cos(f(r_0)t) \qquad (15b)$$

The solution in Eq.(15) is in general <u>not</u> periodic in t ,even though the excitation is periodic with period P. This means that the corresponding trajectory in the $x-y$ plane is not a closed circle as illustrated by the chaotic trajectory calculated with $f(r) = r$, $a = 1.0$, $\omega = \pi$. $(x_0, y_0) = (0, 1.9)$, as shown in Fig. 3.

FIGURE 3

2.3 Poincaré map of the twist-and-flip circuit

The chaotic trajectory shown in Fig. 3(a) shows that even though we can obtain the solution of the twist-and-flip circuit explicitly via Eq.(15), its asymptotic behavior in the $x - y$ phase plane is nevertheless muddled by an infinite tangle of intersections of the trajectory upon itself. The standard method to untangle such a mess of points and extract some useful asymptotic information is to analyze the dynamics of the associated Poincaré map **p** defined as follows [10]: Given any point (x_0, y_0), the Poincaré map of (x_0, y_0) for the twist-and-flip circuit is a point (x_1, y_1) which corresponds to the position of the trajectory from (x_0, y_0) calculated at $t = P = 2\pi/\omega$. Let us denote this map $(x_1, y_1) = \mathbf{p}(x_0, y_0)$ as follows:

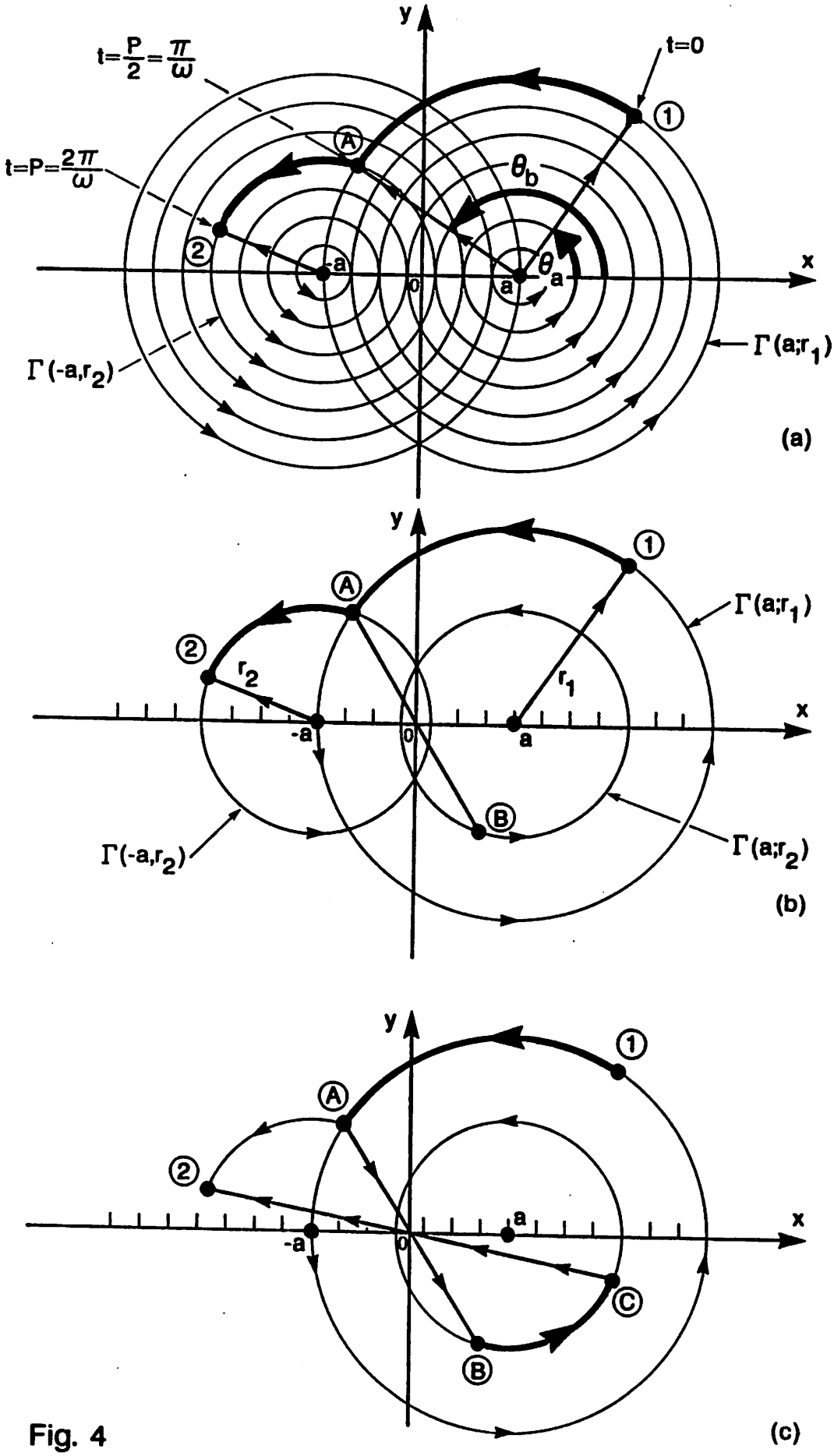

Fig. 4

$$(x_0, y_0) \rightarrow (x_1, y_1) \qquad (16)$$

Let us analyze next the geometrical interpretation of this Poincaré map. Observe first that corresponding to the given initial point ① ($t = 0$) on the outer right circle (centered at $x = a$) in Fig. 4(a), the trajectory traverses this circle in a counterclockwise direction until it arrives at the intermediate point Ⓐ half a period ($P/2 = \pi/\omega$) later. Then it instantly switches to the left family and coasts along the smaller left circle (centered at $x = -a$), still in a counterclockwise direction, until it arrives at point ②a full period ($P = 2\pi/\omega$) later. Hence, in the geometrical construction shown in Fig. 4(a), the Poincaré map (16) can be denoted geometrically by the action:

$$\mathbf{p} : 1 \rightarrow 2 \qquad (17)$$

FIGURE 4

Clearly, we can take point ② as our next initial point and apply the Poincaré map of this point again to obtain ③ This process can be iterated to obtain a sequence of points $(x_0, y_0), (x_1, y_1), (x_2, y_2) \ldots (x_n, y_n), \ldots$.

The loci of these points can be extracted from the mess of points in Fig. 3(a) by applying a regular flash of light (as in a stroboscope) of period $P = 2\pi/\omega$ to obtain a portrait of this chaotic trajectory (assumed hanged on the wall of a dark room). The result is shown in Fig. 3(b).

Observe that the loci of points in Fig. 3(b) actually represents a sequence of points obtained by iterating the Poincaré map of the twist-and-flip map **p**, from one initial point (x_0, y_0). To avoid clutter, however, we will often abuse our terminology by referring to this sequence of points simply as the "orbit from (x_0, y_0)". In examining the gallery of Poincaré maps in section 4, the reader is cautioned that while some of the pictures in this gallery correspond to the orbit of the Poincaré map from only one point, others may contain a union of orbits from the Poincaré map from many initial points, specified in the figure captions. Recall the above Poincaré map **p** of the twist-and-flip circuit consists of the two operations: 1. Given the initial point ① at $t = 0$, identify the radius of that circle centered at $x = a$ which passes

through ① assuming that the initial time corresponds to the beginning of a positive half cycle. This circle is denoted by $\Gamma(a; r_1)$ in Fig. 4(a). Follow the circle in a counterclockwise direction until we arrive at the point labeled ④ where $t = P/2 = \pi/\omega$ (one half of the period of the square wave). We will henceforth refer to this action as a twist T_a relative to the center $x = a$ by an angle $\Delta\theta_1 = \theta_b - \theta_a$. Identify the radians r_2 of the circle centered at $x = -a$ which passes through ④, where the square wave abruptly switches to its negative half circle. This circle is denoted by $\Gamma(-a; r_2)$ in Fig. 4(a). Follow the circle $\Gamma(-a; r_2)$ in a counterclockwise direction until we arrive at the point labelled ② in Fig. 4(a) where $t = P = 2\pi/\omega$ is the period of the square wave. We will henceforth refer to this action as the second twist T_{-a} relative to the center $x = -a$ by an angle $\Delta\theta_2$ where $\Delta\theta_2$ is the angle subtended by the radii from ④ to ②, centered at $x = -a$. It follows from the above geometrical interpretation that the Poincaré map p of the twist-and-flip circuit is made up of two twists T_a and T_{-a}. of angles $\Delta\theta_1$ and $\Delta\theta_2$, respectively. We denote this Poincaré map p by

$$\mathbf{p} = T_{-a} \circ T_a \qquad (18)$$

where "o" denotes the "composition" operation. In terms of this standard mathematical notation, we can write

$$\mathbf{p}(①) = T_{-a} \circ T_a(①) = T_{-a}(④) = ② \qquad (19)$$

For the twist-and-flip circuit, Eq.(19) can be calculated exactly from Eq.(15), and there seems little advantage to resort to the above geometrical construction. However, the same results and phenomena that one finds in the twist-and-flip circuit also occurred in more complicated situations. The simplest example of such a generalization is to replace the gyrator in Fig. 1 by a non-energic two-port resistor [9]. In this case, the two concentric families of circles in Fig. 4(a) are replaced by the concentric non-circular contours centered at $x = a$ and $x = -a$, respectively. These contours can be quite complicated in shape (e.g., topological contours depicting constant elevations in a geographic map) and almost certainly does not have an explicit equation corresponding to Eq.(15). It is in these much more general situations, where the full power of the twist-and-flip circuit as an analytical and tractable paradigm for studying non-autonomous chaos becomes evident. It is in this context that we now make a major conceptual leap forward by showing that

all complicated nonlinear dynamics of the twist-and-flip circuit, as well as its many non-explicit generalizations, can be fully understood by studying an even simpler map, called the twist-and-flip map.

2.4 The twist-and-flip map

The "double" twists actions in Eq. (19) which defines the Poincaré map of the twist-and-flip circuit is summarized geometrically in Fig. 4(b). Suppose we reflect the left circle $\Gamma(-a; r_2)$ with respect to the y-axis and obtain the reflected circle $\Gamma(a; r_2)$ of the same radius r_2 but now centered at $x = a$. Now instead of going from point Ⓐ to point ② by the twist action T_{-a}, we "flip" the point Ⓐ with respect to the origin to obtain point Ⓑ as shown in Fig. 4(b). Note that Ⓑ must necessarily fall on the reflected circle $\Gamma(a; r_2)$. Now instead of applying the second twist action T_{-a} by an angle $\Delta\theta_2$ as in Fig. 4(a), in order to arrive at our desired destination point ②, suppose we repeat the first twist action T_a, now centered at $x = a$, from point Ⓑ by the same angle $\Delta\theta_2$, we would obtain point Ⓒ as shown in Fig. 4(c). Because every point on the left circle $\Gamma(-a; r_2)$ has a corresponding odd-symmetric image (with respect to the origin), it follows that if we "flip" the point Ⓒ in Fig. 4(c) one more time, we should arrive at exactly the same destination point ② defined by the Poincaré map in Eq.(17). If we define this "flip" action by

$$\mathrm{F}\begin{pmatrix} x \\ y \end{pmatrix} = \begin{pmatrix} -x \\ -y \end{pmatrix} \qquad (20)$$

then Ⓑ = F(Ⓐ) = -Ⓐ, and ② = F(Ⓒ) = -Ⓒ. Hence, the above geometrical analysis proves that the Poincaré map (19) for the twist-and-flip circuit is equivalent to the "double" twist-and-flip actions

$$\mathrm{p}(①) = \mathrm{F} \circ \mathrm{T}_a \circ \mathrm{F} \circ \mathrm{T}_a(①) = ② \qquad (21)$$

On first sight, Eq. (21) actually looks more complicated than the original Poincaré map in Eq. (19). Observe, however, that there are two properties in Eq. (21) which we can exploit: First, the flip map F defined by (20) is trivial either geometrically, or numerically. Second, the two twists actions required by Eq. (21) pertain now to only one twist map, centered at $x = a$. If one were to write a computer program to integrate the state equations (5) in order to

identify the locations of points Ⓐ and ② a task needed in the general cases where an explicit solution does not exist, then the algorithm for implementing Eq.(19) would require integrating Eq.(5) over a full period. In contrast, the corresponding algorithm for implementing the equivalent Poincaré map of Eq.(21) would require integrating the state equation twice, each time over a positive half period. The computer program for implementing Eq. (21) is simpler because the same twist action T_a is called upon twice. Observe that there is as yet no savings in the numerical integration time needed to go from ① to ② The key advantage of the equivalent Poincaré map defined by Eq. (21) is best seen by first rewriting it in the following abbreviated form

$$\mathbf{p} = \mathrm{FTFT} = (\mathrm{FT})^2 \qquad (22)$$

where we have dropped the subscript a from T, since we no longer have to distinguish T_a from T_{-a}, as would be the case in Eq.(19). Hence, we have simplified the Poincaré map p of the twist-and-flip circuit, or its non-circular and possibly damped generalizations, to the double action of a single map

$$\Phi = \mathrm{FT} \qquad (23)$$

henceforth called the twist-and-flip map [3]. Now since all nonlinear dynamical phenomena and complexities exhibited by the Poincaré map p in Eq.(22) are also present in the twist-and-flip map and vice-versa, it suffices to study Φ in so far as the qualitative behavior of the twist-and-flip circuit is concerned. This observation has great advantages: In the geometrical interpretation of Fig. 4(b), this means that we need only analyze the properties of the map from an initial point ① to its single twist-and-flip image point Ⓑ For the much larger class of "generalized" (possibly with damping) twist-and-flip circuits, having no explicit solutions, this observation allows the construction of a simplified Poincaré map Φ which consumes half the computing time required for the full Poincaré map p.

3 Properties of the Twist-and-Flip Map

As noted in section 2 the twist-and-flip map has numerous mathematical properties that allow an extensive analysis of its complexity and also allow the possibility of designing circuits with predetermined characteristics. In this

section we will state without proof some of these properties. Before describing these properties we present some preliminaries essential to understanding the properties of the twist-and-flip map and to understanding the fractals and fractal-like structures presented in the later sections.

3.1 Preliminary Concepts

In this subsection we will describe certain important concepts from Hamiltonian dynamics for a mapping Φ that have an enormous bearing on the formation of fractals in the twist-and-flip circuit. The concepts we will describe are those of elliptic and hyperbolic fixed points, invariant regions, elliptic regions, stable and unstable manifolds, homoclinic tangles, and KAM island chains. Each of these objects plays an interesting role in the complex dynamics of chaos through the way they contribute to the formation of fractals and fractal-like structures in the twist-and-flip circuits.

Fixed Points and Periodic Points: A fixed point p of an invertible and differentiable mapping Φ of the plane $\mathbf{R}^2$ is one such that $\Phi(p) = p$. A period-two point for Φ is a point p such that $\Phi(\Phi(p)) = p$. This last line is usually abbreviated as $\Phi^2(p) = p$. A period-n point of Φ is a point p such that $\Phi^n(p) = p$. Thus a period-n point of Φ is a fixed point of Φ^n.

Invariant Regions: Given a map Φ of $\mathbf{R}^2$, a region or subset of $\mathbf{R}^2$, call it Λ, is said to be invariant for Φ if $\Phi(\Lambda) = \Lambda$.

This last condition means that given any point $q \in \Lambda$, $\Phi(q)$, which need not be equal to q, remains inside Λ. Conversely, given any point $q \in \Lambda$, there is some point $q^* \in \Lambda$ such that $\Phi(q^*) = q$.

Area Preserving: Give a map Φ which is differentiable we denote its derivative at the point p as $\mathrm{D}(\Phi)(p)$. If $\mathrm{D}(\Phi)(p) = 1$ for all p in the plane, then Φ is called area preserving. When referring to systems, a term often used for area preserving is nondissipative. Area preserving means that if we start with a square with area 1, then Φ will map this region to another region (which usually is not another square) having area 1.

Elliptic Points: For an area preserving map Φ, a fixed point of Φ is called elliptic if the Jacobian derivative matrix, denoted $\mathrm{D}(\Phi)$ of Φ has eigenvalues on the unit circle [7], p.305. A fixed point of an area preserving map Φ is called hyperbolic if one eigenvalue of the Jacobian at the fixed point is

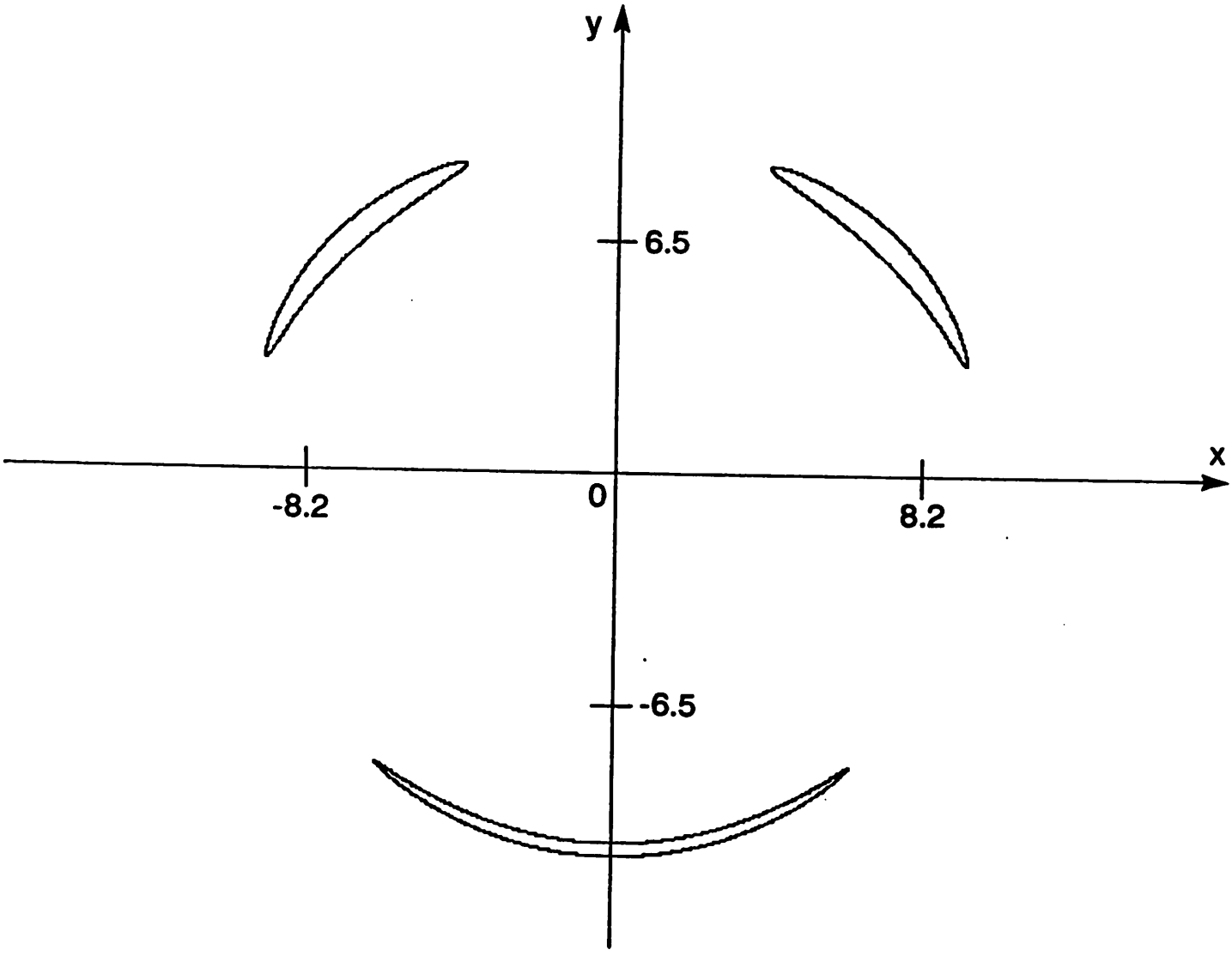

Fig. 5(a)

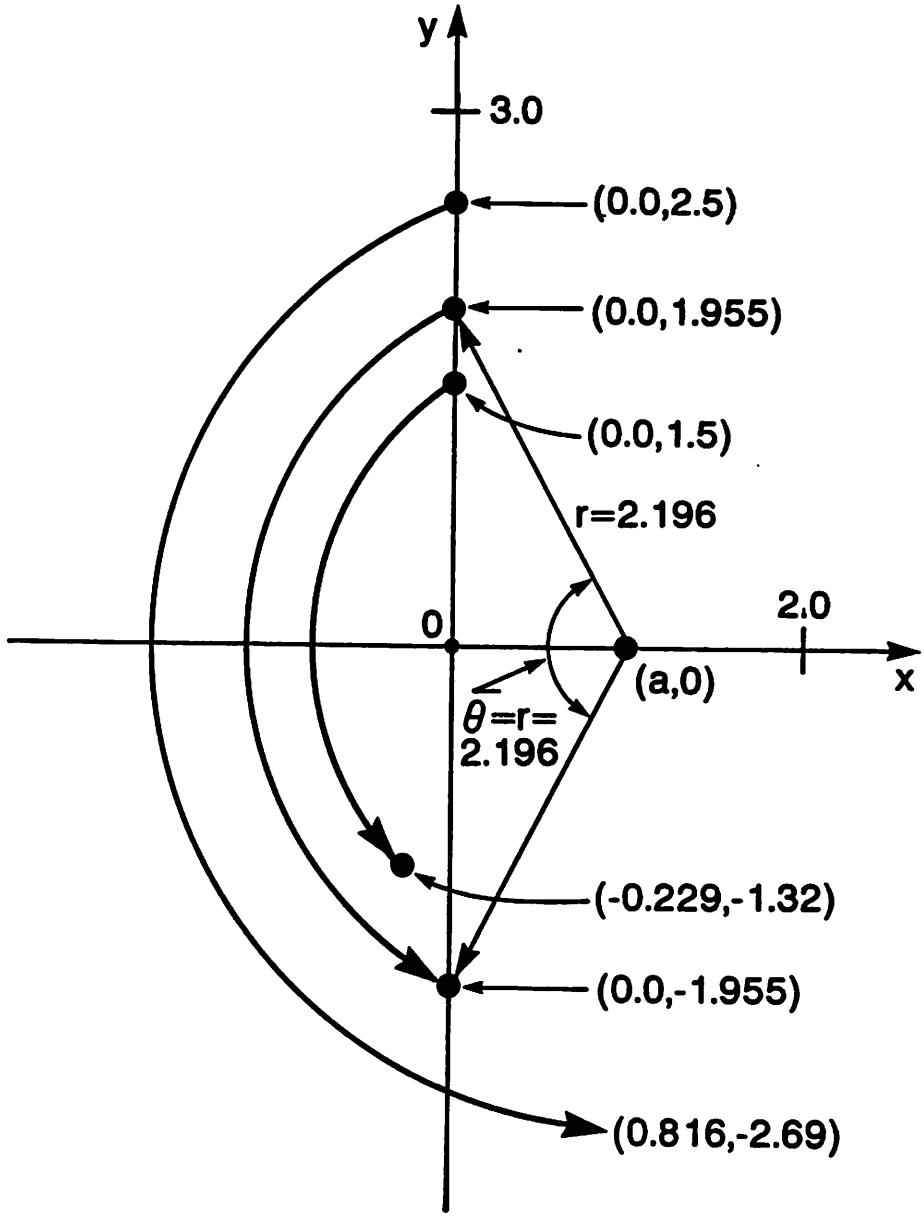
y
3.0
(0.0,2.5)
(0.0,1.955)
(0.0,1.5)
r=2.196
0
2.0
(a,0)
x
θ=r=
2.196
(-0.229,-1.32)
(0.0,-1.955)
(0.816,-2.69)

Fig. 5(b)

greater than one in absolute value and the other is less than one in absolute value.

FIGURE 5

If we consider a point near an elliptic fixed point, the set of iterates of this point will, for the mappings we will be considering, seem to trace out a closed curve if we iterate the point enough times. See Fig. 5(a). The time waveform of the corresponding differential equation is a quasi-periodic function in the sense that it behaves much like a function which is a finite sum of periodic functions having incommensurate frequencies. A sum of continuous periodic functions having incommensurate frequencies is referred to in the mathematical literature as "almost periodic".

Stable and Unstable Manifolds: Passing through a hyperbolic fixed point, sometimes called a saddle point, there are two special curves called the stable and unstable manifolds respectively [7], p.68. These curves are invariant in the sense that any iterate of any point on either of these curves will remain on the respective curve.

The stable manifold is so called because if we start at a point on the stable manifold and iterate our map Φ it will converge, i.e., approach, the fixed point. For the unstable manifold, this does not happen. In fact, for a point very near the fixed point and on the unstable manifold, its iterates by Φ will move away from the fixed point. Such points may also temporally move toward the fixed point and then move away, or may from time to time come near the fixed point. To get around this clumsy explanation of the unstable manifold in terms of Φ we use Φ^{-1} instead, where Φ^{-1} denotes the inverse of the Poincaré map which exists because Φ is defined by a differential equation. When we do the definition gets easier: We define the unstable manifold as the set of points which approach the fixed point under iteration by Φ^{-1}. So that the stable manifold for Φ is the unstable manifold for Φ^{-1} and vice versa. An important fact about these two curves is that neither curve can intersect itself. This follows from the uniqueness of solutions of ordinary differential equations and we do not give the exact argument here. However, these curves can intersect each other, i.e., the stable and unstable manifolds can actually intersect. Further, these two curves may coincide completely.

When the stable and unstable manifolds intersect by crossing at a single point the result is chaos.[7], p.165.

The easiest example available to understand these ideas it that of the 2×2 matrix

$$\begin{bmatrix} 2 & 0 \\ 0 & 1/2 \end{bmatrix}$$

Its inverse is the matrix

$$\begin{bmatrix} 1/2 & 0 \\ 0 & 2 \end{bmatrix}$$

(0, 0) is a fixed point of this matrix when the matrix is considered as a mapping on the plane and points on the $y-$axis converge to (0, 0) under forward iteration of this map. Hence, the entire $y-$axis is the stable manifold. Points on the $x-$axis converge to (0, 0) under iteration by the inverse matrix, and hence the entire $x-$axis is the unstable manifold. In this instance the stable and unstable manifold are straight lines. When our maps are nonlinear, such as the twist-and-flip map, these two special sets are curves that often wind around in the plane in a most extraordinary manner, as can be seen in the examples found in [6], pages 406,407. A particularly simple example can be found on p.410, Fig.5. We will present additional examples in section 4.

The significance of the stable and unstable manifolds is that they may be used to produce fractals which are Cantor sets. These particular fractals are of considerable importance in understanding the dynamics of systems that can be described by differential equations. How this is done can be found in section 11.5 of [6]. These Cantor set fractals generally cannot be seen on a computer, but their existence can be proved [7], p.165 and it is this set of "invisible" fractals that is the source of the most complex form of chaos produced by fractals. In fact, the only definitive statement that has ever been made about the level of complexity that can occur in a mapping arising from a differential equation is about the maps generating these type of fractals and it is known as the Smale-Birkhoff theorem. The Smale-Birkhoff theorem does not use the term "fractal" since the Smale-Birkhoff theorem predates the use of the term "fractal".

The stable and unstable manifolds can be associated to other fractals as will be seen in a later section.

The conventional symbols used to denote an unstable or stable manifold are as follows:

The Unstable Manifold of a mapping Φ at a fixed point p is denoted $W^u(p)$; the stable manifold is denoted as $W^s(p)$.

Note that since a period-n point, p, of a mapping Φ is a fixed point of Φ^n, Φ^n also has a stable and unstable manifold when p is hyperbolic. Further, when p is hyperbolic for Φ^n, each of the points $\Phi^k(p)$, $k = 1, 2, 3 \ldots n$ is also fixed by Φ^n and has a stable and unstable manifold. Hence there are n stable and unstable manifolds for a period-n point, each a separate curve.

A fixed point is synonymous with a period-one point.

Homoclinic Tangles: As described in [7], p.165 the stable manifold and unstable manifold can curve around so extensively they actually become tangled in one another. Figure 3.32 of [7] on page 165 is a drawing of such a tangle and Fig.9 of [5], page 248, is an actual picture of such a tangle from a twist-and-flip map. Such tangles are referred to in the literature as *homoclinic tangles.* We do not attempt to explain the genesis of this term. Wherever there are homoclinic tangles, the Smale-Birkhoff theorem tells you there is chaos which is related to Cantor set fractals.

Island Chains: Given a map Φ which defines a non-dissipative (area preserving) system, the elliptic and hyperbolic periodic points of Φ provide an organizing structure within which its dynamics may be best understood. In particular, there is the interesting phenomena known as island chains where there exist a set of alternating elliptic and hyperbolic periodic points of the same period that seem to form in a ring. Around the elliptic periodic points of period-n are regions which are invariant (i.e. a subset of positive area which is a continuum in which each point defines a quasi-periodic orbit) for Φ^n. In this sense they are like islands in that if one starts iterating Φ^n in one of these regions, you will never leave while the intermediate iterates, $\Phi, \Phi^2, \Phi^3, \ldots, \Phi^{n-1}$ will jump from from one region to the next. Surrounding these islands are homoclinic tangles of stable and unstable manifolds. A picture of a set of these islands will show that they form in a circle like shape, much like a ring of mushrooms sometimes forms in the forrest. Figure 6.18, p.340 of [7] is a highly stylized drawing of such an island chain. Of course real island chains are not so neat. The circular formation of these islands has come to be called an *island chain* due to its similarity to the shape of a chain. In section 4 we will illustrate these island chains using the twist-and-flip map and we will see that they are not so neatly formed as the drawing of [7]. But for now we note only that their complexity is enormous

and diverse and has a self-similar aspect in that within an island of an island chain can be found another island chain of smaller scale, and so on, much the same as occurs in fractals. For this reason we refer to an island chain as a fractal-like structure.

In summary, we have described the concepts of elliptic and hyperbolic fixed points, invariant regions, elliptic regions, stable and unstable manifolds, homoclinic tangles, and island chains. In the following sections we will see that each of these objects plays an interesting role in the complex dynamics of chaos through the way they contribute to the formation of fractals and fractal-like structures in circuits. In particular, with the addition of small amounts of damping to the twist-and-flip map as would naturally occur in actual implementation of the circuit equations, the complexity spawned by these features of Hamiltonian dynamics actually shape the final form in which fractals occur as well as their contribution to the formation of chaos in nonlinear circuits. It is the possibility of utilizing these features in the design of new generation of systems, neural networks, and computers that makes their understanding imperative.

3.2 Twist-and-Flip Properties

The matrix form of the twist part of the twist-and-flip map, T, is given by:

$$\mathrm{T}\begin{pmatrix} x \\ y \end{pmatrix} = \begin{bmatrix} \cos(f(r)\pi/\omega) & -\sin(f(r)\pi/\omega) \\ \sin(f(r)\pi/\omega) & \cos(f(r)\pi/\omega) \end{bmatrix} \begin{pmatrix} x-a \\ y \end{pmatrix} + \begin{pmatrix} a \\ 0 \end{pmatrix}$$

which represents a counter clockwise rotation about the center $(a, 0)$ by an angle equal to $\pi\, f(r)/\omega$ For $f(r) = r$ we have the simple twist-and-flip map. The matrix representation (matrix form) of the twist-and-flip mapΦ = FT is the mapping obtained by multiplying the right hand side of

$$\mathrm{T}\begin{pmatrix} x \\ y \end{pmatrix}$$

above by -1. We often consider the special case where $f(r) = r$ and will henceforth refer to is as the simple twist-and-flip map

We now list and explain some properties of the twist-and-flip map which can be found in [5] and [6]:

Property 1: If $f(r)$ is a strictly increasing function, then FT has an infinite number of fixed points. Moreover, they all lie on the vertical axis and approach infinity in both directions. In particular these fixed points lie on the intersection of the vertical axis and the curves defined parametrically by [13]:

$$\begin{aligned} x(t) &= a \pm t\,\cos(0.5\pi\, f(t)/\omega) \\ y(t) &= \mp t\,\sin(0.5\pi\, f(t)/\omega) \end{aligned}$$

for $0 \leq t < \infty$, where the upper (resp. lower) sign pertains to the first (resp. second) curve, called control manifolds [6]. If $f(t)$ is a positive increasing function, then these curves are spirals and so must cross the vertical axis infinitely many times.

Another method of seeing this fact is to set $\mathrm{FT}(x,y) = (x,y)$ and solve this set of equations to get:

$$\begin{aligned} \cos(\pi f(r)/\omega)) &= 2(a/r)^2 - 1 \\ \sin(\pi f(r)/\omega) &= 2ay/r^2 \end{aligned}$$

As $r \rightarrow \infty$ these equations are:

$$\begin{aligned} \cos(\pi f(r)/\omega)) &\approx -1 \\ \sin(\pi f(r)/\omega) &\approx 0 \end{aligned}$$

and so there may be solutions for which $f(r) \approx 2n\omega$. If $f(r)$ is increasing and continuous it will actually reach $2n\omega$ for every n and thus also have infinitely many solutions near $2n\omega$, each solution corresponding to a fixed point of FT.

To see that these solutions must be on the vertical axis we note that the condition $\mathrm{FT}(x,y) = (x,y)$ requires that the distance from $(a,0)$ to the fixed point and the distance from $(-a,0)$ to the fixed point must be the same. This means that $(x-a)^2 + y^2 = (x+a)^2 + y^2$, or that $x = 0$.

By using an illustration it can be easily seen that some points on the vertical axis will be fixed by FT. In Fig. 5(b), we show where three points on the vertical axis are mapped by the simple twist. The highest point on the vertical axis is $(0.0, 2.5)$. Its image under the twist map overshoots the

vertical axis and arrives at the point (0.816, -2.69) (we have added the circular arcs between each point and its image under the simple twist map in Fig. 5(b) to facilitate the explanation). The flip of this point is (-0.816, 2.69) which is not equal to the starting point. The image under the simple twist of the point (0.0, 1.5) is not carried far enough and arrives at the point (-0.229, -1.31). The flip of this point is also not equal to the starting point. Note that when the value of the y-component of the starting point is 2.5 the x-component is positive, when the value of the y-component of the starting point is 1.5, the x-component is negative. Since the gyration conductance function is continuous, there must be some y-value of a starting point on the vertical axis between 1.5 and 2.5 where the x-component of the image of this point under the simple twist takes on the value 0.0. This value can approximated either by trial and error, or by using a Newton iteration algorithm, and is found to be ≈ 1.9551 which is accurate to about six decimals.

Property 2: $\det(\mathrm{D(FT)}) = 1$, for all x, y, where D(FT) is the Jacobian derivative of FT.

Property 3: The trace of D(FT) at a hyperbolic fixed point is given by

$$\mathrm{tr} = 2(1 + \frac{ayg'(r)\pi}{r\omega}) - 4(\frac{a}{r})^2$$

and $\mathrm{tr} > 2$ for $y \geq 2\omega/\pi$. Due to property 2 the product of the eigenvalues is one and hence all fixed points for which $y \geq 2\omega/\pi$ along the positive y-axis are hyperbolic saddle points and therefore have stable and unstable manifolds.

In order to produce the unstable manifold on a computer we need the following fact:

Property 4: For a hyperbolic fixed point of FT on the vertical axis the expanding eigenvector of the unstable manifold has a slope given by

$$\mathrm{slope} = -\frac{a}{y}\sqrt{\frac{(\mathrm{tr}/2)+1}{(\mathrm{tr}/2)-1}}.$$

In order to produce the stable manifold on a computer we need the following three facts:

Property 5: The flip map F can be factored into two reflections, PR, where P is reflection about the horizontal axis and R is reflection about the

vertical axis. Using this notation we have the following property, called the *involution* property, of the twist-and-flip map:

PTPT = I. Thus, $\mathbf{PT} = (\mathbf{PT})^{-1}$

Property 6: As a result of the involution property we have the following fact: $\mathbf{RFT} = (\mathbf{FT})^{-1}\mathbf{R}$.

In mathematical terminology, this means that the twist and flip map is topologically conjugate [7] to its inverse through reflection about the vertical axis.

From the above two properties we have the following result that allows us to easily generate the stable manifold, once the unstable manifold has been generated:

Property 7: Given a hyperbolic fixed point, p, of FT, let $W^s(p)$ be the stable manifold, and let $W^u(p)$ be the unstable manifold at this fixed point. Then $\mathbf{R}(W_p^u) = W_p^s$. This means that if (x, y) is a point on the unstable manifold, then $(-x, y)$ is a point on the stable manifold and vice versa. Hence the unstable manifold is identical to the reflection of the stable manifold about the vertical axis. This includes the possibility that $W^u(p) = W^s(p)$ a possibility that was mentioned earlier. In this case there are no places where the stable and unstable manifold intersect in only one point since they intersect everywhere. In this case there is no chaos caused by these unstable manifolds since there can be no homoclinic tangles. A necessary and sufficient condition for the existence of homoclinic tangles is that there exist at least one place where the stable and unstable manifolds cross at a single point. When this occurs, there will be many other crossings of this type and hence a homoclinic tangle will exists. Thus we may clarify our definition of homoclinic tangles by saying that homoclinic tangles exist when there exist numerous, (infinitely many will exist, but we do not prove this) places where the stable manifold and unstable manifold cross at a single point. This crossing may be tangential so long as an actual crossing occurs.

This definition suggests that it will be useful to have some simple test for the presence of homoclinic tangles in the twist-and-flip map. This test is given below as property 8. In the following we use $[x]$ to denote the integer part of x and use r_0 to denote $2\omega[r/2\omega]$.

For a simple twist-and-flip map we have the following test to determine

the existence of homoclinic tangles, and their associated fractals.

Property 8: *Given a hyperbolic fixed point* $(0, y)$, *with* $r = \sqrt{y^2 + a^2}$ *and* $r_0 = 2\omega[r/2\omega]$, *a sufficient condition for the simple twist-and-flip map to have a homoclinic tangle is that the two circles,*

$$(x - a)^2 + y^2 = r_0^2$$

and

$$(x + a)^2 + y^2 = r^2$$

intersect.

Another form of this condition is given by the following inequality:

$$r \leq 2a + r_0$$

or

$$r \bmod (2\omega) \leq 2a.$$

4 Gallery of Fractals

In this section we will illustrate a variety of fractals and fractal-like structures that occur in the twist-and-flip map. We will use an indirect method to illustrate these fractals similar to the method used to illustrate the $1/3^{rd}$ Cantor set [11]

The fractals occurring in the twist-and-flip map are of four types. Those associated with an attractor, those associated with a homoclinic tangle, those associated to the boundary of a set of elliptic regions, and cantori. Due to the extent to which the fractals associated with attractors and homoclinic tangles have been studied, we will confine our attention to the fractals from boundaries of elliptic sets and cantori. In addition to fractals, we will also examine some fractal-like structures. We do this since the role of these fractal-like structures in creating dynamic complexity is every bit as important as the dynamic complexity arising from fractals. These fractal-like structures, as mentioned in subsection 3.1, are referred to KAM island chains and are organized around a remarkable combination of elliptic and hyperbolic periodic points. What these structures have in common with fractals is that they occur on all scales and their complexity continues to unfold without apparent limit as a given region of the phase plane is subject to ever increasing

levels of magnification. Island chains differ from fractals in that they are not known to be self-similar and there is no simple way to associate a fractional dimension to them.

All of the figures in this section are of the phase plane Poincaré map explained in the previous sections. This section is primarily organized around the gyration conductance function of the twist-and-flip circuit due to its physical significance as a circuit element.

4.1 Class A: Gyration conductance function $f(r) = r$

The gyration conductance function, $f(r) = r$, corresponds to the simple twist rotation function. We begin with an illustration of the fractal-like KAM island chains occurring in the twist-and-flip map having this gyration conductance function. This Hamiltonian type of dynamic phenomena has been studied for years by the use of the Henon map [12] or the standard map [7]. What has only recently been discovered is that this phenomena can be associated to a circuit. See Fig. 6(a), where $a = 1.0$, $\omega = \pi$. The center point of the yellow, inner most region is (0.0, 6.2031) and is elliptic of period-two. As seen in this figure, there is a complex invariant set of elliptic regions (closed curves) and homoclinic tangles (in orange) that represent the array of possible outputs of the circuit. We pause for a moment here to clarify the term *elliptic region*. Elliptic regions are regions around elliptic periodic points in which, for every point in the region, the solution of the differential equation or the output of the circuit is quasi-periodic. These regions may be small or large depending on the particular parameters of the circuit and gyration conductance function f that appears in the circuit. Hyperbolic regions are more difficult to explain. For the purposes of this paper we will consider a hyperbolic region to be the union of the stable manifold and the unstable manifold from the same hyperbolic periodic point. The boundary separating the elliptic and hyperbolic regions (when homoclinic tangles exist) cannot be seen in this figure due to the difficulty of producing it on a computer. We conjecture that it is a fractal. One way to see this is to note that the boundary of an elliptic region tries to be quasi-periodic since its points are very close to points giving rise to quasi-periodic outputs of the circuit. But such points are equally near to points on a stable or unstable manifold which produces chaotic outputs of the circuit. Hence the boundary points are simultaneously influenced by order (quasi-periodic motion)

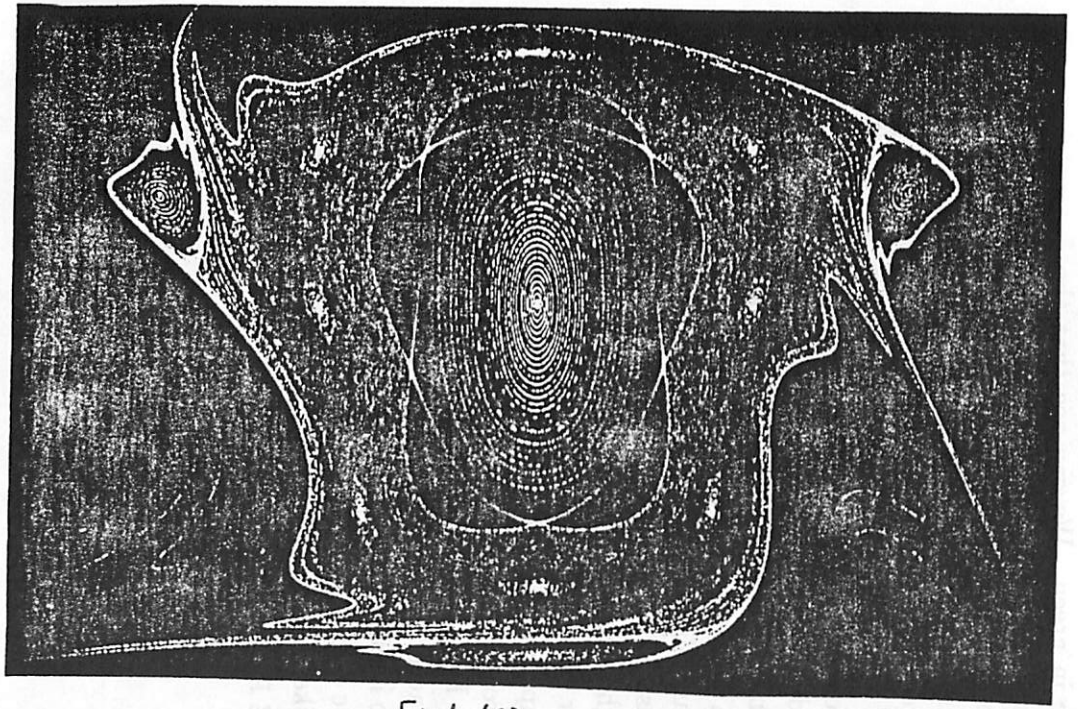

Fig 6 (a)

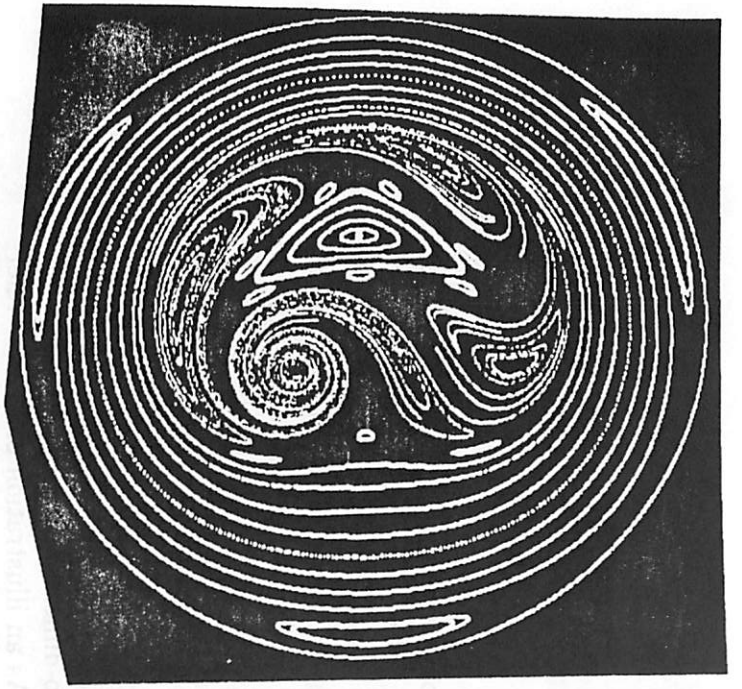

Fig 7 (a)

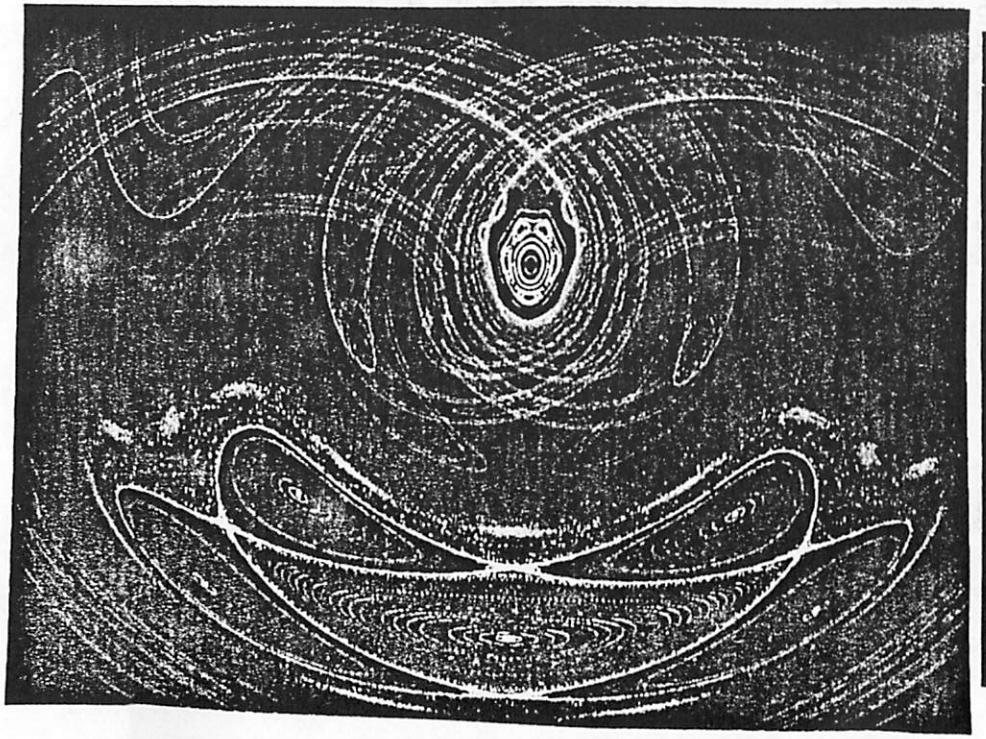

Fig 6(b)

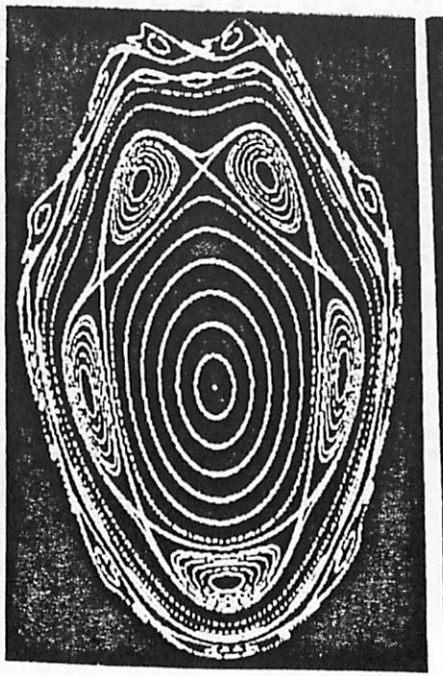

Fig 6 (c)

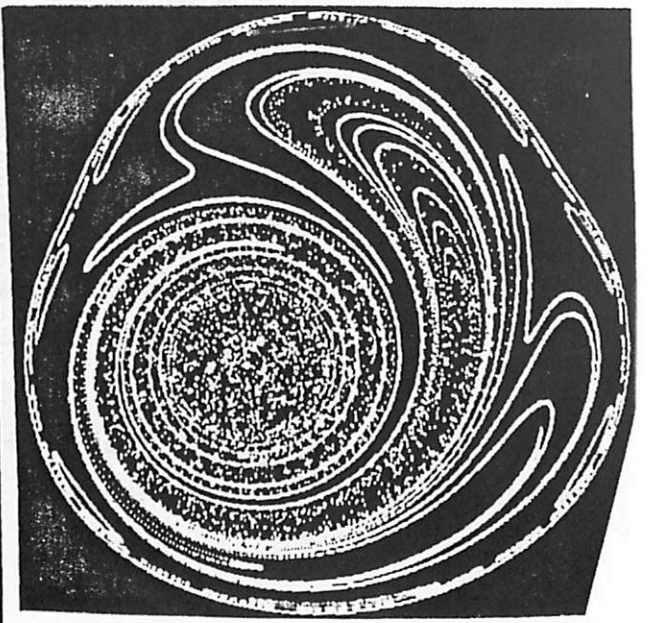

Fig 7 (c)

and chaos (the homoclinic tangles). This boundary must be an invariant set since the elliptic and hyperbolic regions are both invariant. What we expect is points on this boundary behave for some period of time like points in the elliptic region and then for some time like points in the hyperbolic region. Perhaps some are altogether different. Only a very strange set could support such diverse behavior and hence we conjecture it must be fractal. If it were possible to use a point on this fractal boundary as input values to the circuit, the output would be unpredictable.

The pedagogical value of the twist-and-flip circuit can be readily appreciated when one considers that every known form of dynamical complexity, Hamiltonian or dissipative, that arises in two-dimensional dynamical systems can be found in the twist-and-flip circuit. As an illustration of this we refer the work of Henon [12] and others summarized in [7].

For example, Fig. 6(a) shows the twist-and-flip dynamics that corresponds to Fig.1.40, page 53 of [7] as-well-as p.309 of Henon [12]. Figure 6(b) is an example of an extensive homoclinic tangle in green. We can see that the figure is vertically symmetric. A fixed point is located at $(0.0, 1.955)$ and is the fixed point of Fig. 5(b). This fixed point is located at the intersection of the two thickest parts of the green curves, in the middle (measured from the sides) of the figure and above the yellow region. This homoclinic tangle is a detailed illustration of the complexity of a tangle and corresponds to the more modest hand-drawn figure, Fig.3.35, found in [7] on page 170. Fig. 6(c) corresponds to Fig.3.36, page 171 of [7] and is an enlargement of the yellow region in Fig. 6(b). The center of the inner most elliptic regions is the elliptic fixed point $(0.0, 0.69898)$. This Fig. 6(c) is a good example of the relationship of elliptic and hyperbolic regions in the phase plane known as island chains. The elliptic regions are "centered" whereas the hyperbolic regions are the colored regions that seem to diffuse through the elliptic regions. If we were to magnify a small portion of a region near the hyperbolic period-11 point, $(0.0, 1.341)$, we would continue to see complexity unfold on all scales. An enlargement of the homoclinic tangle in red at this hyperbolic period-11 point at the top of Fig. 6(c) corresponds to Fig. 1.42, page 55 of [7].

The most significant aspect of this extraordinary complexity is that the twist-and-flip circuit provides a window into its study through the twist-and-flip map. Being able to harness this dynamic complexity in the design of new systems, circuits, or neural networks will likely lead to a new generation of novel applications, possibly unlike anything presently known.

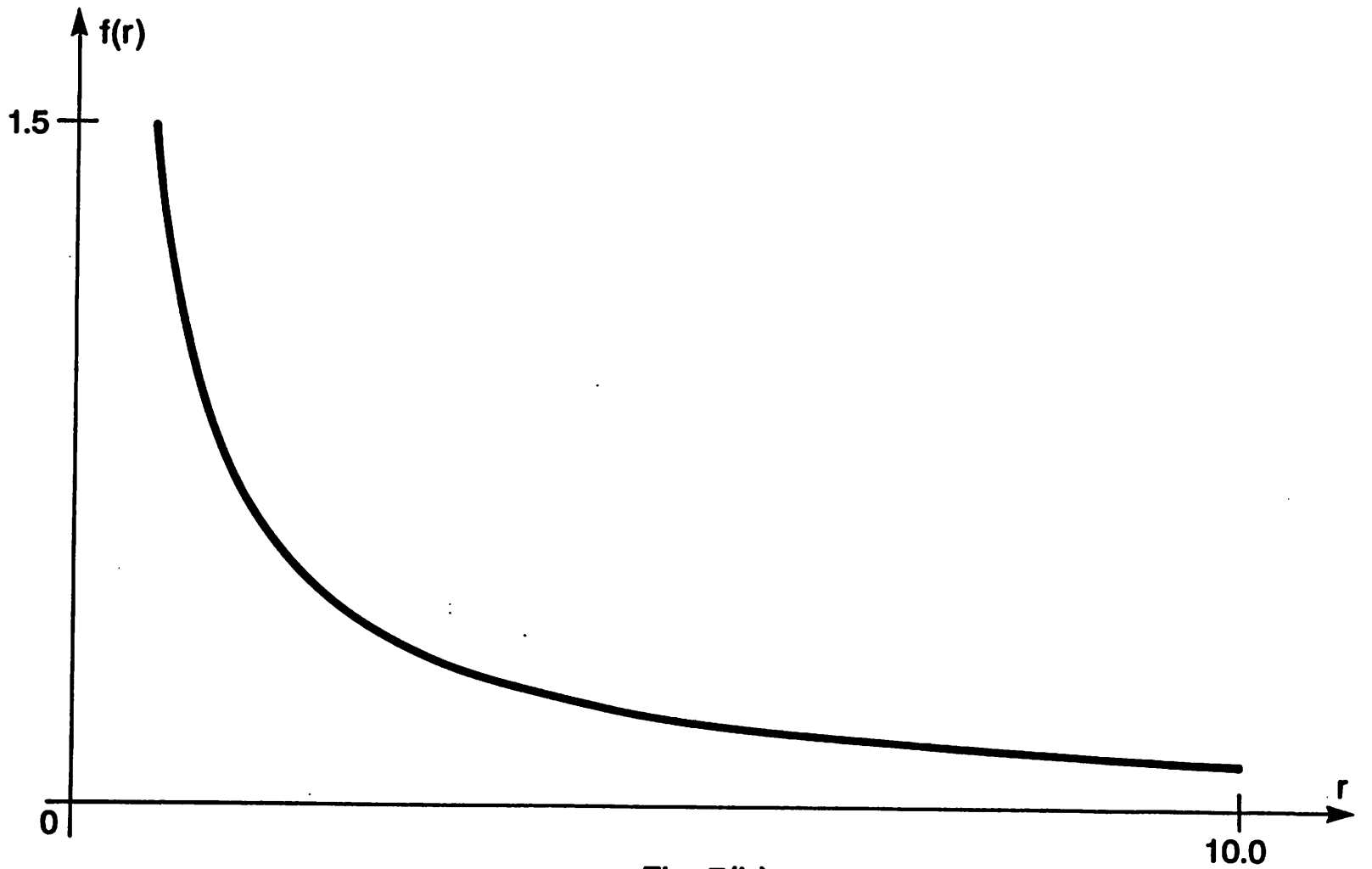

Fig. 7(b)

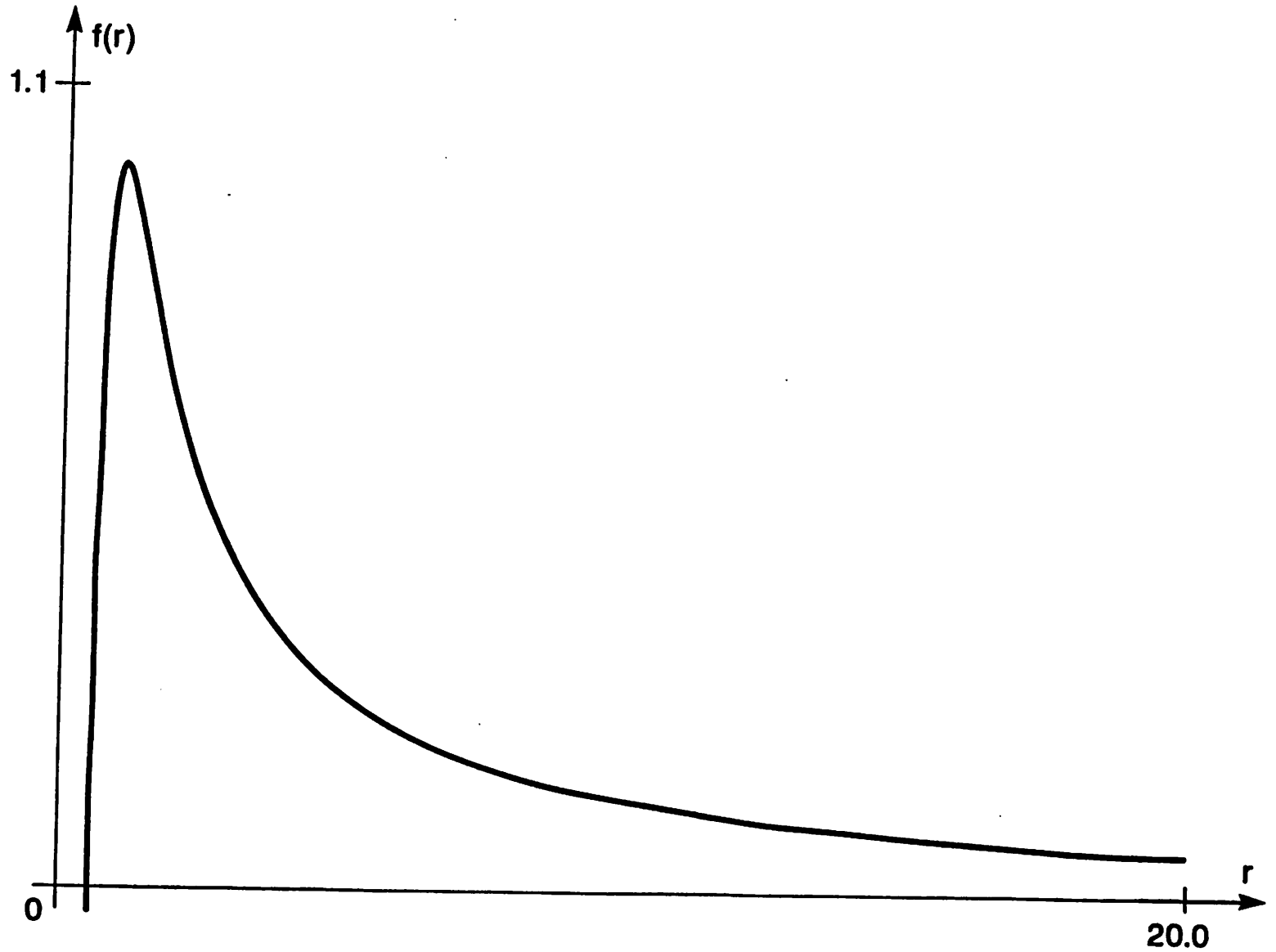

Fig. 7(d)

4.2 Class B: Gyration conductance function $f(r)$ is continuous and positive

It is an important fact to note that the twist-and-flip circuit has a range of dynamic diversity far beyond that found in either the standard map or the Henon maps. Both the maps of Henon and the standard map have parameters that allow a broad range of experiments to be conducted. But the twist-and-flip circuit does also through the physically meaningful parameters a,ω. Further, it has the gyration conductance function, $f(r)$. To see that the dynamic diversity due to this feature opens an additional dimension to experimentalist we present two figures of the elliptic and hyperbolic regions determined by varying the gyration conductance function. Additional examples can be found in [6]. For a gyration conductance function $f(r) = 1/r$, $a = 0.2$, and $\omega = \pi$ we have Fig. 7(a). For this map there exist a period-9 point located at (0.0, 0.13414). Fig. 7(a) shows the unstable manifold in blue, a set of elliptic regions in the interior in red, and another set of elliptic regions in green surrounding the unstable manifold. Fig. 7(b) is the graph of the gyration conductance function.

FIGURE 7(b) and (d)

In Fig. 7(c) the gyration conductance function is $f(r) = (r + \log(r))/r^2$, $a = 0.2$, and $\omega = \pi$. A hyperbolic fixed point is located at $(0.0, 0.318218)$. In this figure a blue unstable manifold corresponding to this hyperbolic fixed point is shown inside an elliptic region which is in green. Also inside this green elliptic curve are two sets of smaller elliptic curves shown in magenta and red so that they may be easily distinguished. Fig. 7(d) is the graph of this gyration conductance function.

4.3 Class C: Gyration conductance function $f(r)$ is step-wise constant (stair-case) and positive

In this section we use a stair-case type gyration conductance function to illustrate a fractal boundary that naturally occurs in the twist-and-flip circuit. The construction is similar to that used in the illustration of the $1/3^{rd}$ Cantor set.

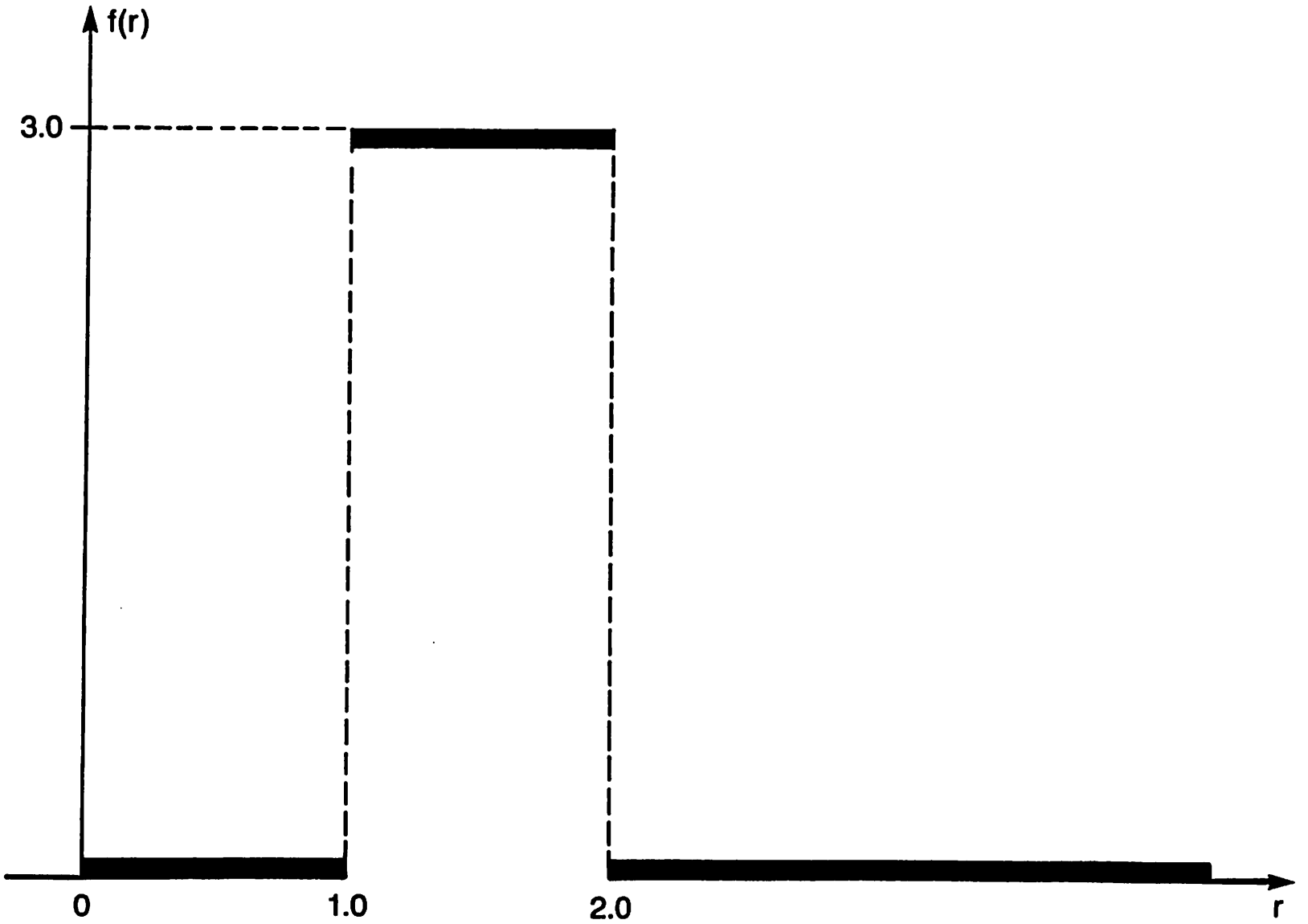

Fig. 8(a)

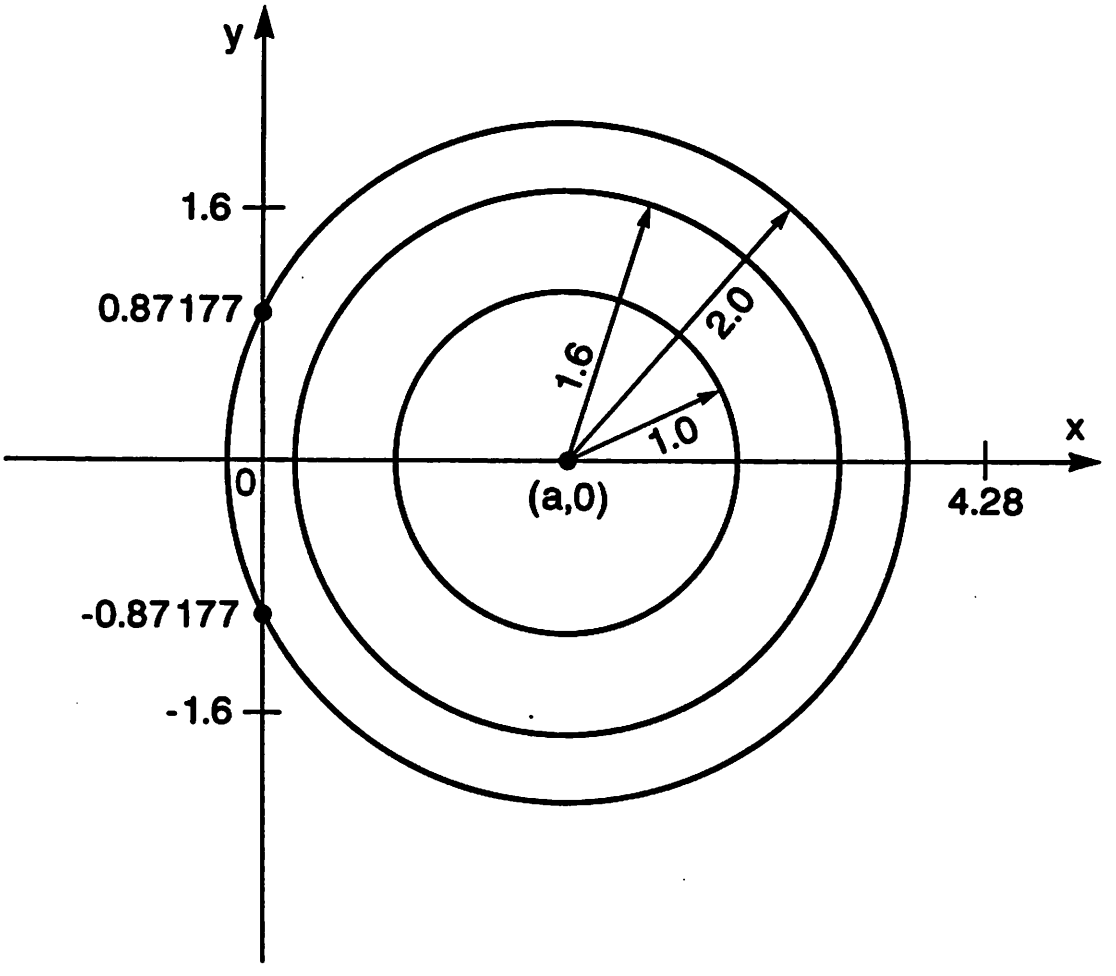

Fig. 8(b)

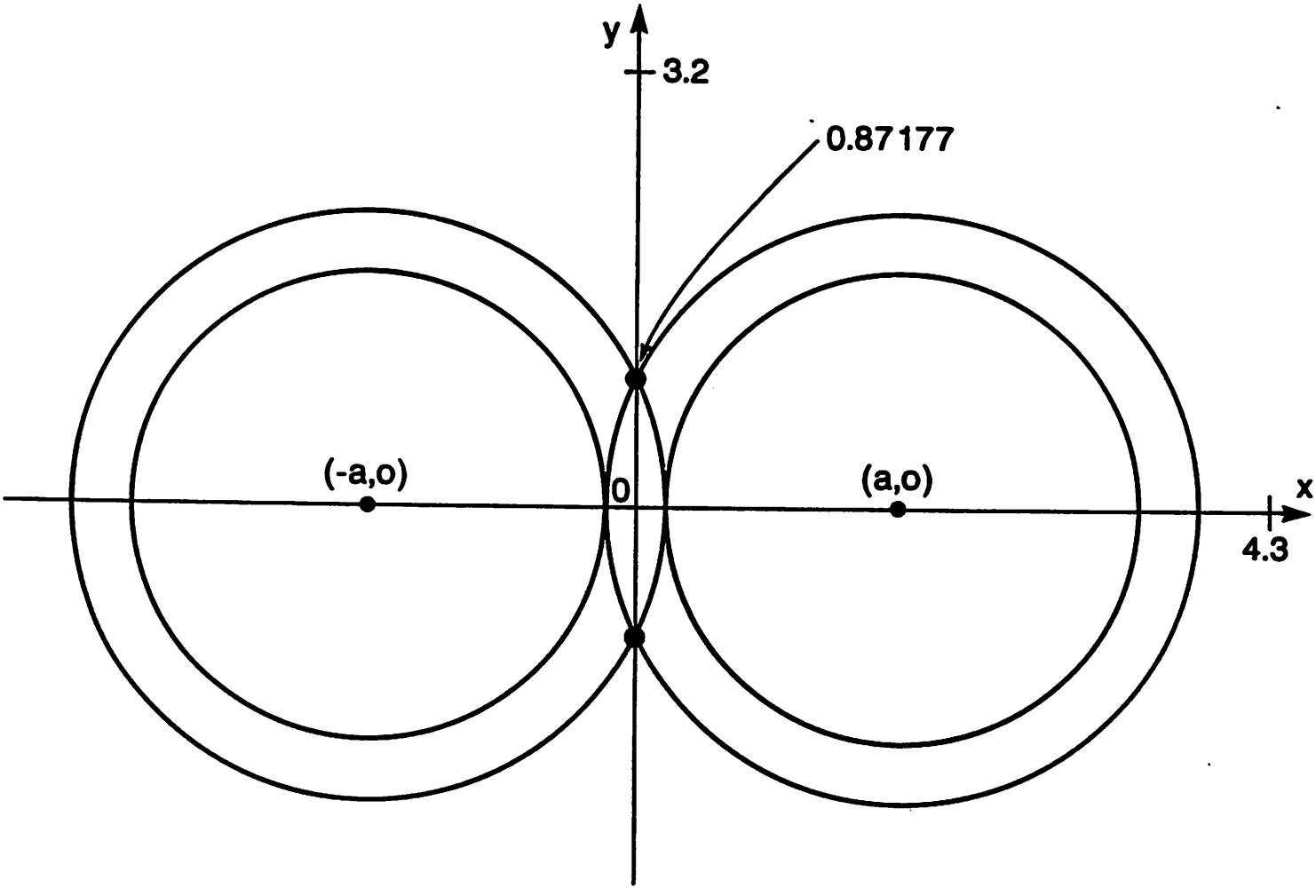

Fig. 8(c)

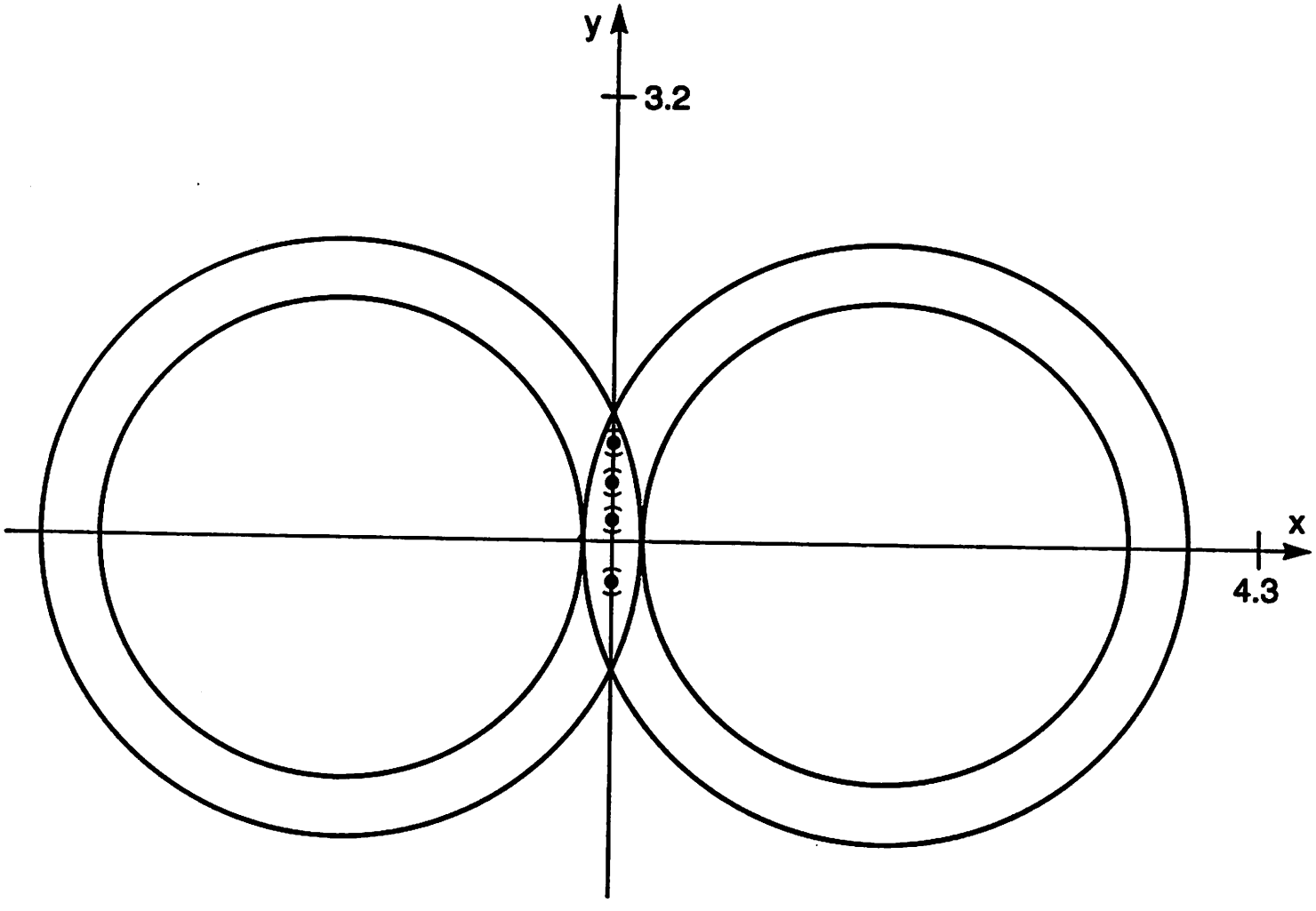

Fig. 8(d)

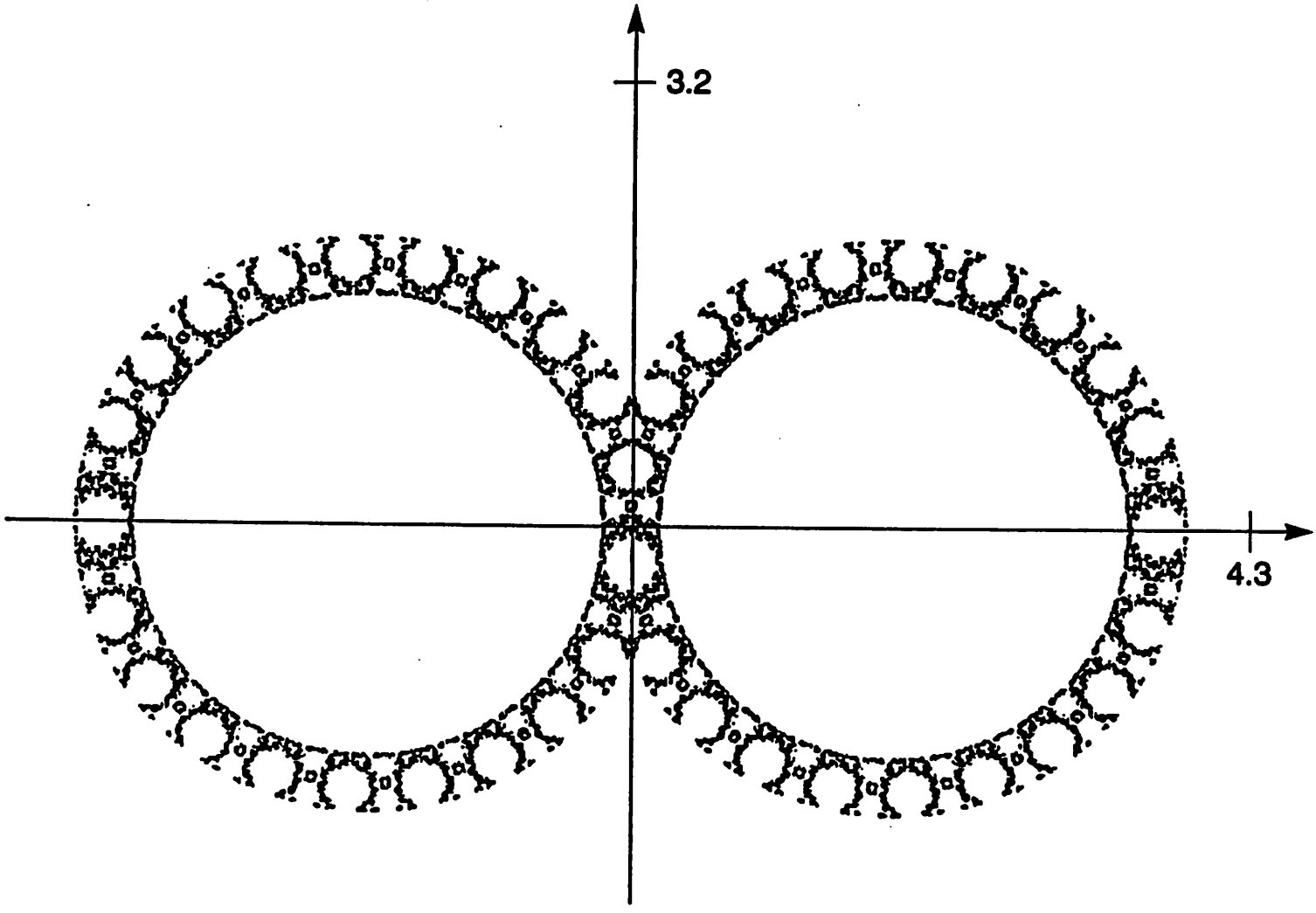

Fig. 8(e)

FIGURE 8(a) through (d)

The gyration conductance function is

$$0.5r_0\ (\mathrm{sgn}(r-1) - \mathrm{sgn}(r-2))$$

$a = 1.8$, $\omega = \pi$, and $r_0 = 3.0$. The graph of this function is seen in Fig. 8(a). As seen there $f(r)$ is 0.0 from 0.0 to 1.0. It is 3.0 for $1.0 < r < 2.0$, and is 0.0 for $2.0 \leq r$. This graph represents the degree of rotation present in the twist function centered at the point $(a, 0.0)$ in the phase plane. See Fig. 8(b). Starting at $(a, 0.0)$, and going out to the circle of radius of 1.0 the twist has 0.0 rotation. Hence T fixes every point inside the inner circle in Fig. 8(b). Between the inner circle and the outer circle, T rotates every point 3.0 radians, and outside the outer circle of radius 2.0, T fixes every point as well. As a result of this gyration conductance function, the entire dynamics of this circuit takes place on a region that is the union of two annuli. See Fig. 8(c). (Our thanks to Professor Morris W. Hirsch for suggesting this map.) The point where the two outer circles intersect on the positive vertical axis is $y = 0.87177$. The intersection of these two circles on the negative vertical axis occurs at $y = -0.87177$ We are going to focus our entire attention on the vertical line between these two points.

By a geometric argument that we will omit we can prove that a point of period-three can be found at $(0.0, -0.2565836)$. The following formula is derived from that argument and can be used to find any values of y_0 such that $|y_0| \leq 0.87177$ and $(0.0, y_0)$ is periodic of period-n and all of the periodic points lie on two circles, one centered at $(-a, 0.0)$ and the other centered at $(a, 0.0)$, with the same radius:

$$y_0 = a\ \tan(\theta)$$

where θ is given by the formula

$$\frac{((n+1)/2)r_0 \bmod (2\pi)}{2}$$

and $n = 1, 3, 5, 7, \ldots, 2k-1$.

For any n for which there is a solution to this equation with $|y_0| \leq 0.87177$, there is an elliptic periodic point of period-n on the vertical axis for FT.

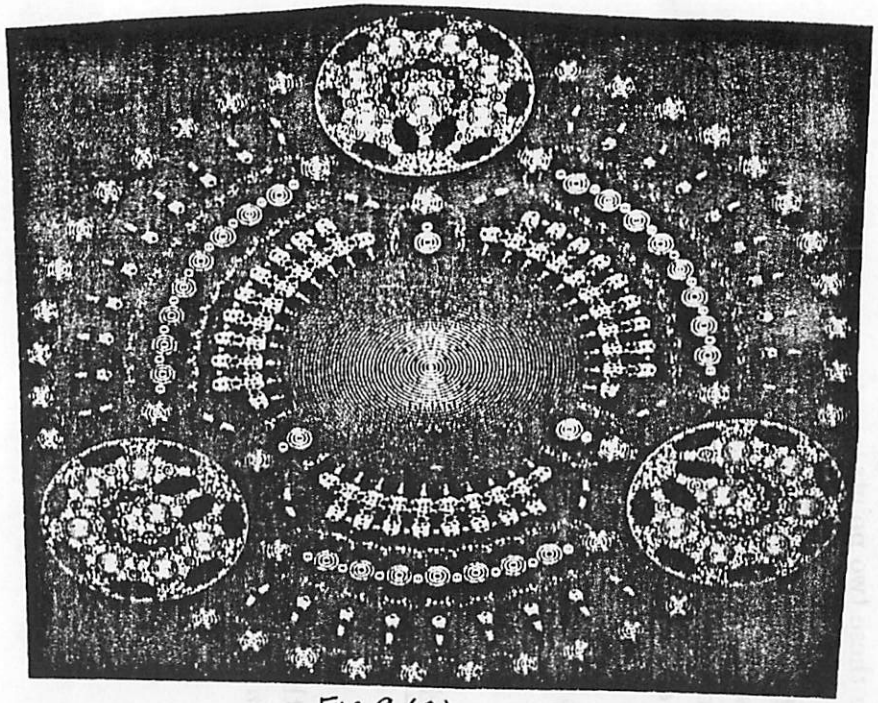

Fig 9 (a)

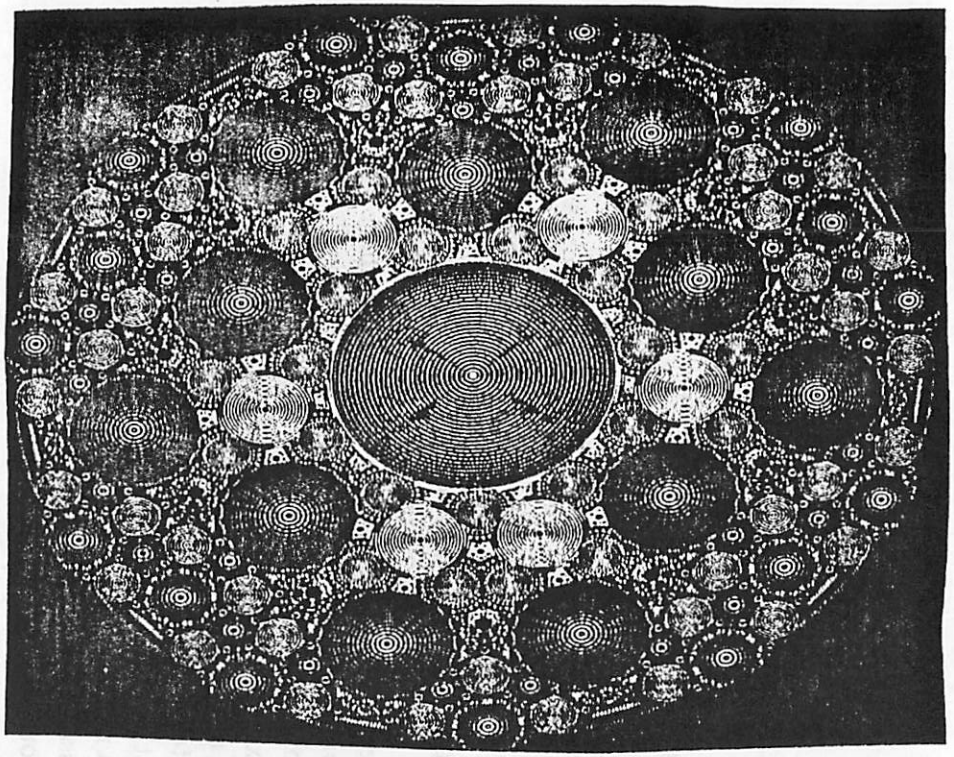

Fig 9 (b)

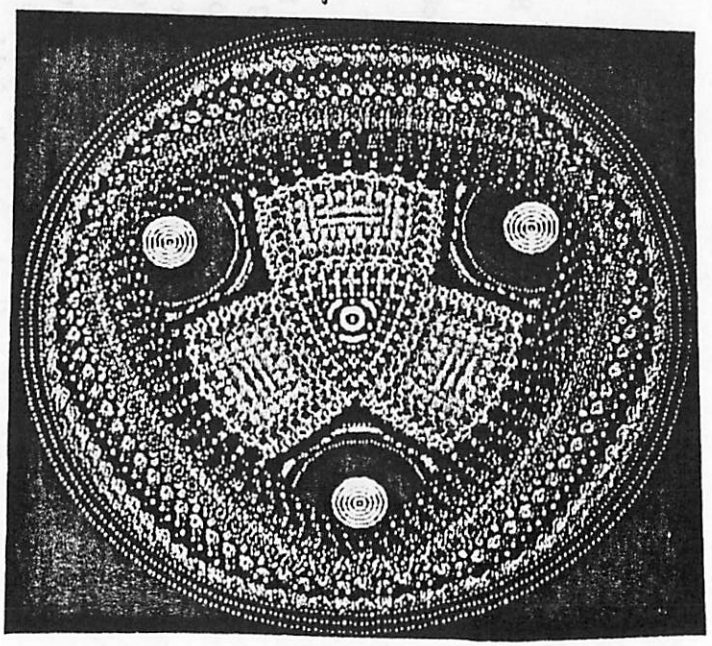

Fig 9 (c)

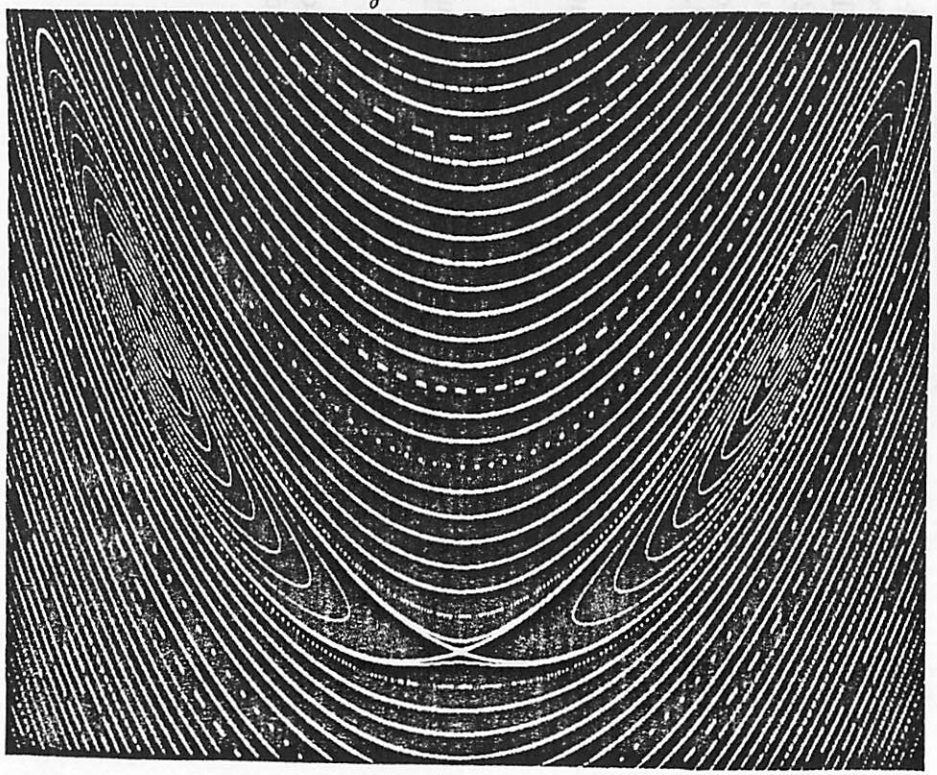

Fig 10 (b)

Using this formula we can find elliptic periodic points of period 3, 33, 37, and 41 on the vertical axis between the limits -0.87177, and 0.87177. The periodic points are of the form $(0.0, y_0)$, where y_0 is obtained from the above formula. For example, for the period-33 point we have $y_0 = 0.69248$.

Around each elliptic point of period-n exist a largest region, invariant under the map $(\mathrm{FT})^n$, which is a circle. The intersection of this circle with the vertical axis is an interval. If we remove these intervals, we have the start of the construction used to generate the $1/3^{rd}$ Cantor set. See Fig. 8(d).

To continue this construction we generate additional elliptic periodic points by the use of even more complex formulae which we do not present here. For example there are periodic points of periods 47, 63, 100 that cannot be generated with the above formula. We remove the largest interval around these points as before. If we continue in this manner, only the boundary of these intervals remains, which is a Cantor set and thus a fractal. The forward and backward iterates of this fractal by FT is still a fractal and the union of all of these iterates is the fractal boundary of the union of all of the elliptic regions in the annulus. In order to see what this fractal looks like we refer to Fig. 8(e). What we see in this figure is not actually the fractal, but a very good approximation to the fractal which is in fact a periodic orbit of FT of very high period that we have not determined.

Another method of visualizing this fractal is to fill in all of the elliptic regions, and then the fractal is what would be left over. But this can only be done in an approximate sense. We refer ahead to Fig. 13(a) which illustrates seven sets of elliptic regions that arise from the seven periodic points mentioned above. Each region is in fact a connected set in the shape of a circle but the figure only shows asterisk shaped regions for computational convenience. Since the twist-and-flip map preserves area, all of the regions of approximately the same size are related. In particular, in the center of each circle is a periodic point, and the number of related regions of the same size is equal to the period of this point. For example there are 37 of the largest yellow regions. At the center of each region is a point of period-37 (there are also some small unrelated yellow regions). There are 3 of the largest magenta, or reddish-purple, regions, each containing a point of period-three at its center. We have generated only seven sets of these elliptic regions, but there are infinitely many more. Each set of regions is composed of a number, say n, of connected disks having a periodic point of period-n at its center. We cannot prove this at this time but we conjecture that every connected

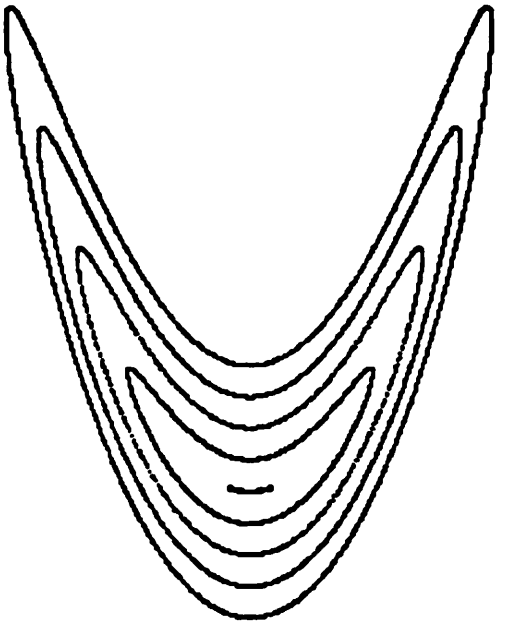

Fig. 10(a)

disk lying within the union of the two annuli seen in Fig. 13(a) contains a periodic point of period-k, and hence a maximal connected disk which is mapped onto itself by the k^{th} iterate of FT. The k iterates of this maximal connected disk are all of the same area and form an open set such as the sets of disks seen in Fig. 13(a).

Fractals of this type (boundaries of elliptic regions) are unlimited in the twist-and-flip circuit. Figure 9(a) has gyration conductance function:

$$f(r) = \begin{cases} 0.5 & \text{for} \quad r < 1.0 \\ 2.0 & \text{for} \quad 1.0 \leq r \leq 2.0 \\ 1.0 & \text{for} \quad r > 2.0 \end{cases}$$

and $a = 5.0$ and $\omega = \pi$.

Figure 9(b) has gyration conductance function:

$$f(r) = \begin{cases} 1.0 & \text{for} \quad r < 1.0 \\ 2.0 & \text{for} \quad 1.0 \leq r \end{cases}$$

where $a = 1.0$ and $\omega = \pi$

Figure 9(c) has gyration conductance function:

$$f(r) = \begin{cases} 1.0 & \text{for} \quad r < 1.0 \\ 1.1 & \text{for} \quad 1.0 \leq r \leq 2.0 \\ 1.0 & \text{for} \quad r > 2.0 \end{cases}$$

where $a = 1.0$ and $\omega = \pi$.

We remind the reader that what is seen in these figures is not the actual fractal, but something like its outline. If we try to imagine the boundary of all of these elliptic regions, that boundary would be the fractal.

5 Using the twist-and-flip circuit to illustrate the effects of perturbations on KAM circles

In this section we illustrate two KAM phenomena using the twist-and-flip circuit. The first is the breakup of elliptic regions and KAM circles by a

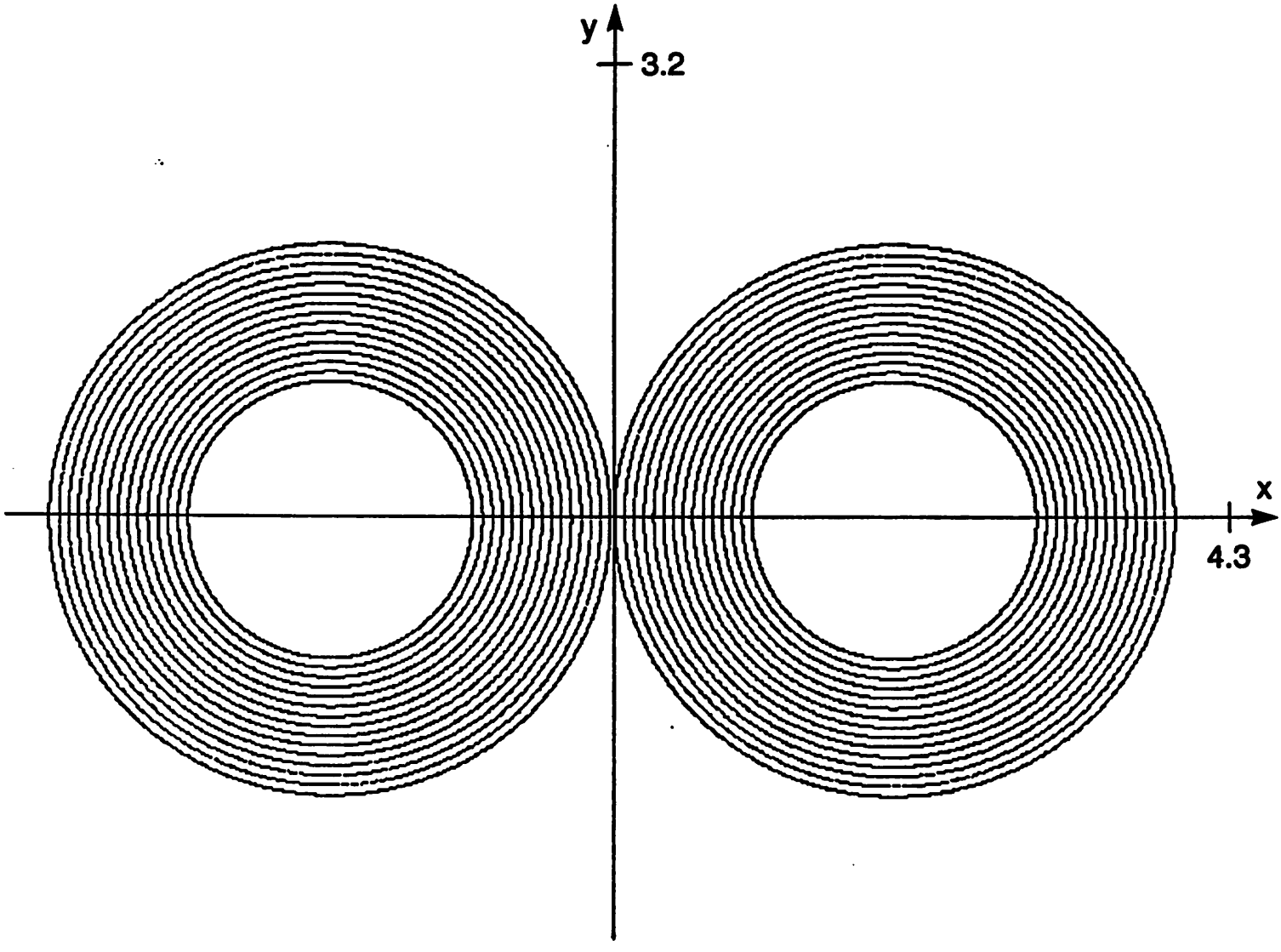

Fig. 11(a)

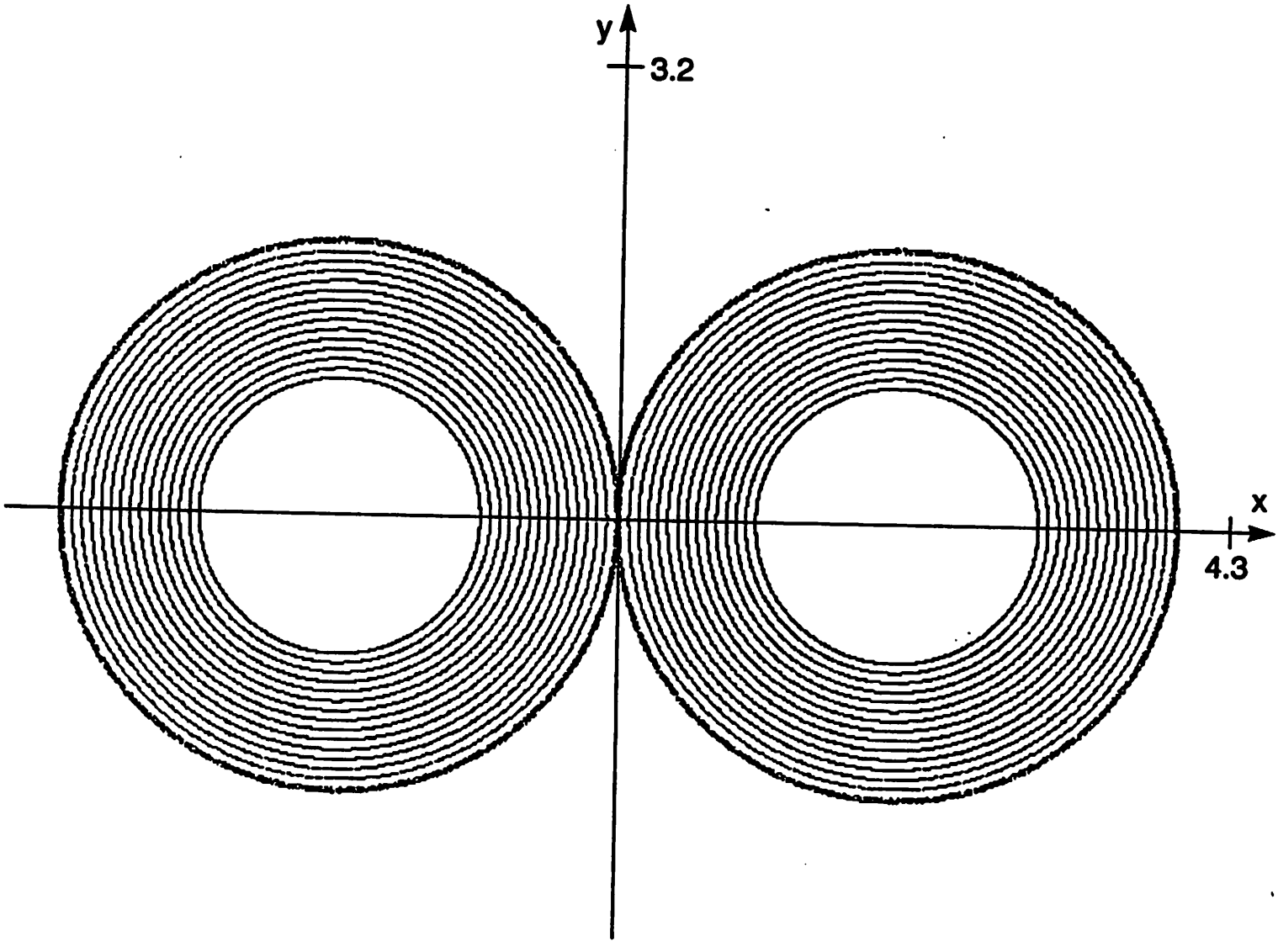

Fig. 11(b)

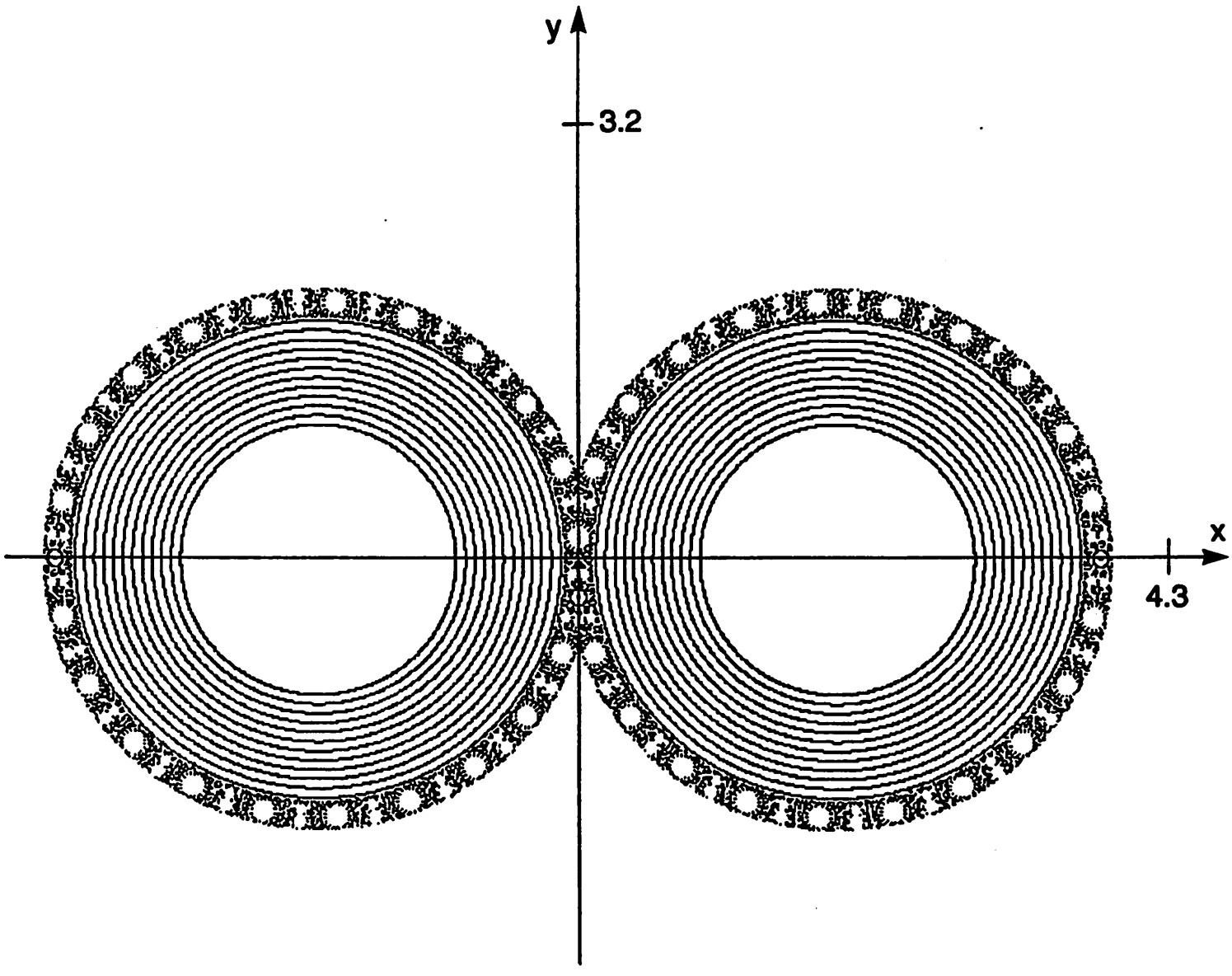

Fig. 11(c)

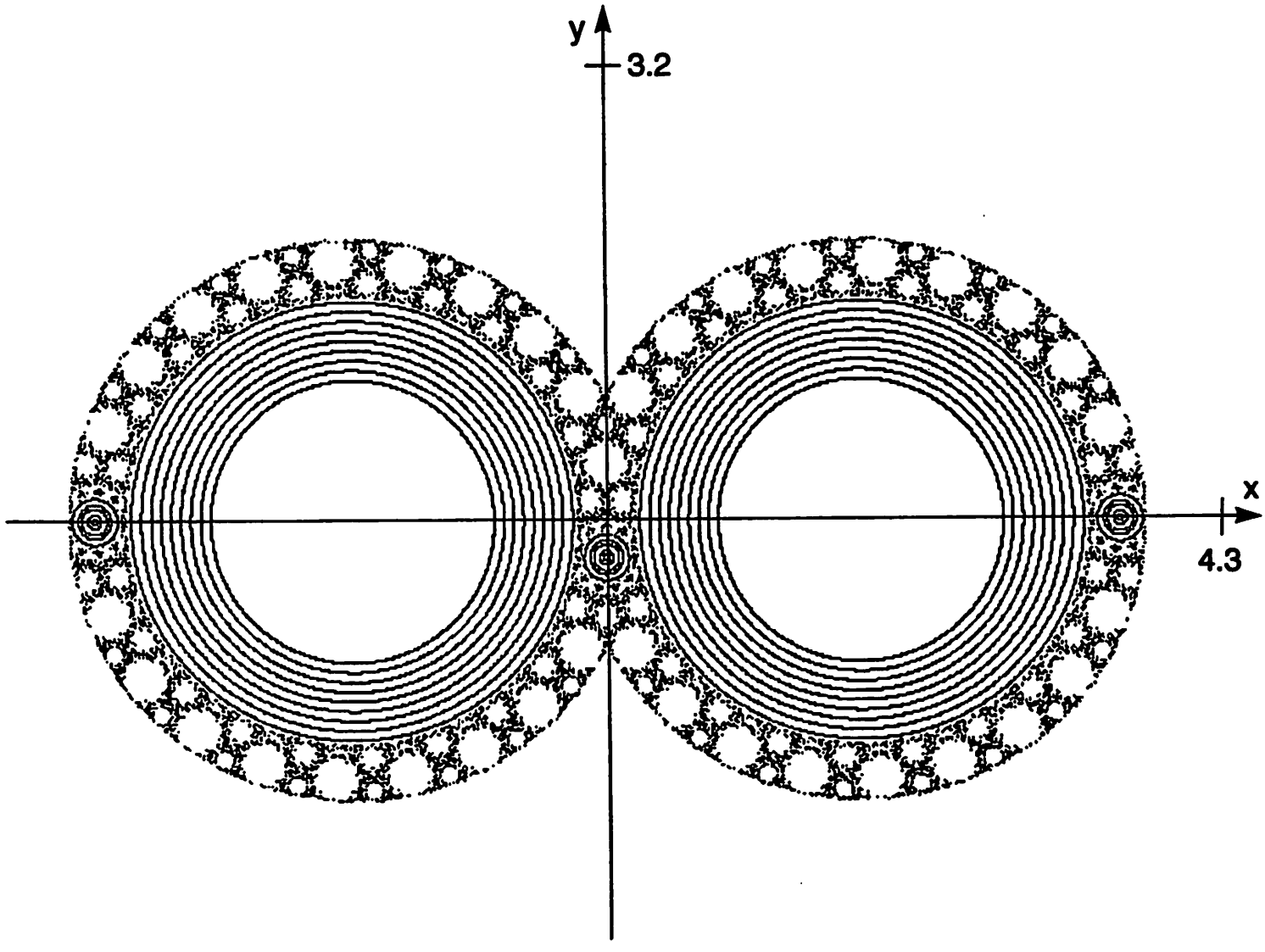

Fig. 11(d)

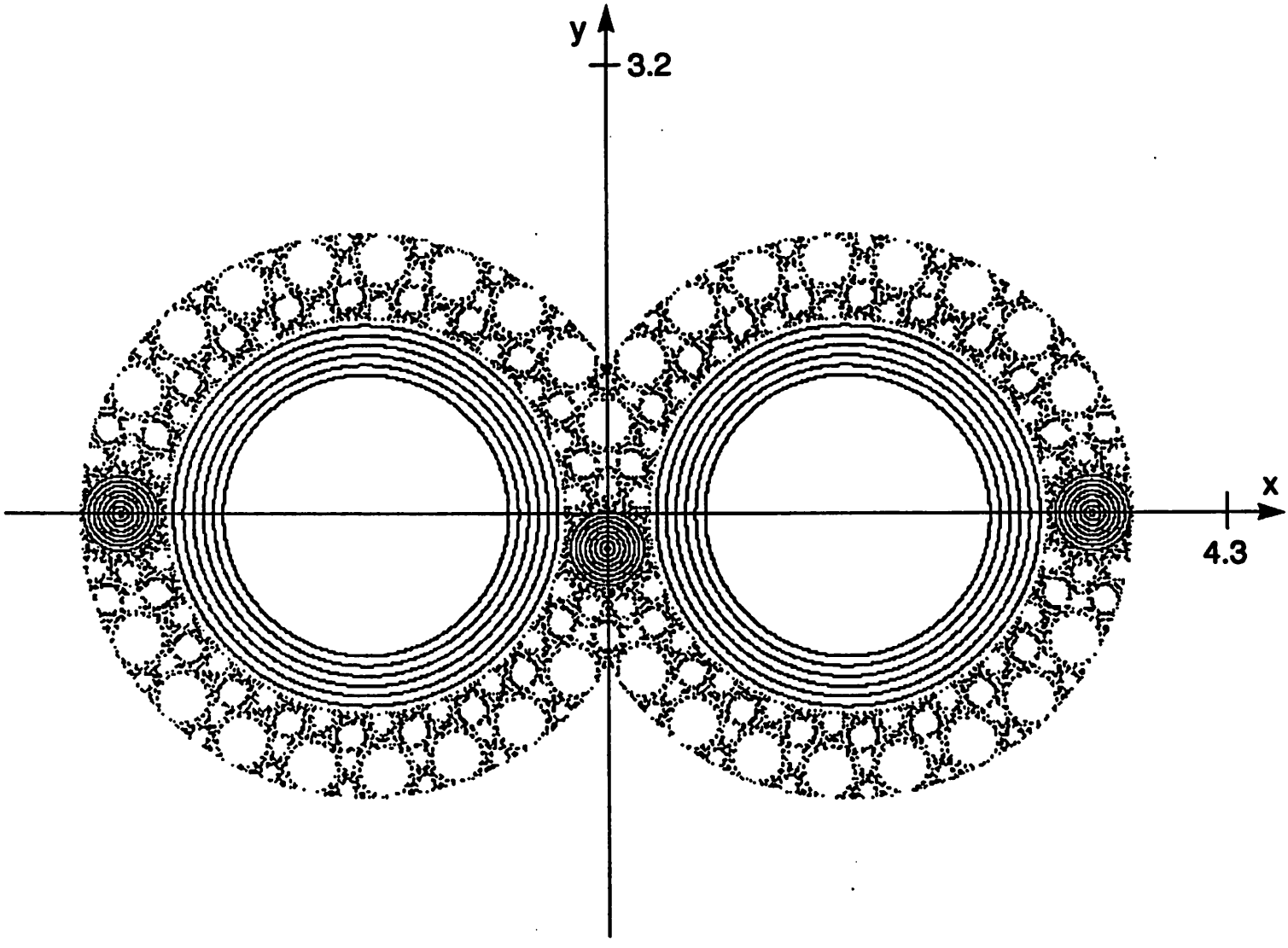

Fig. 11(e)

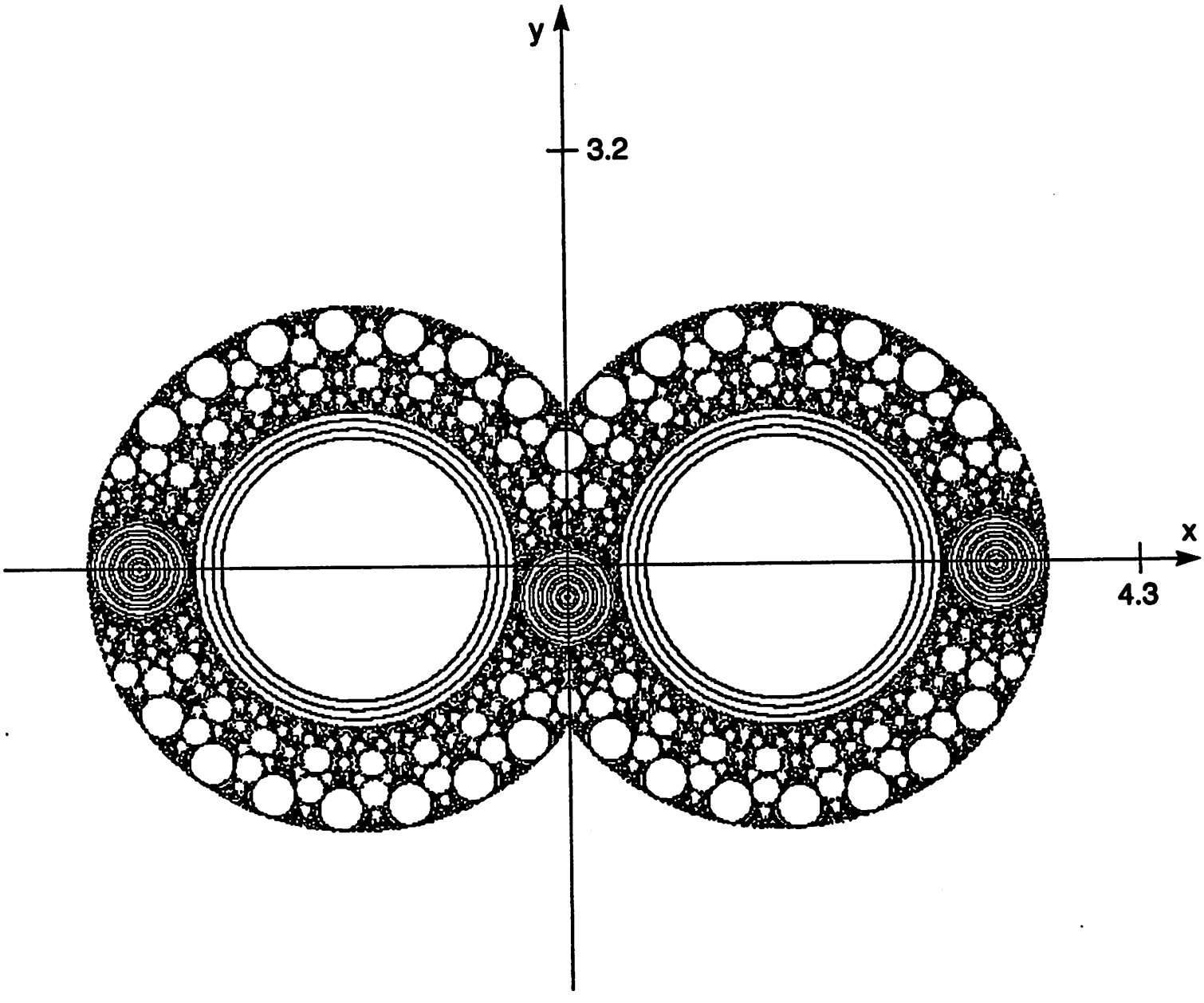

Fig. 11(f)

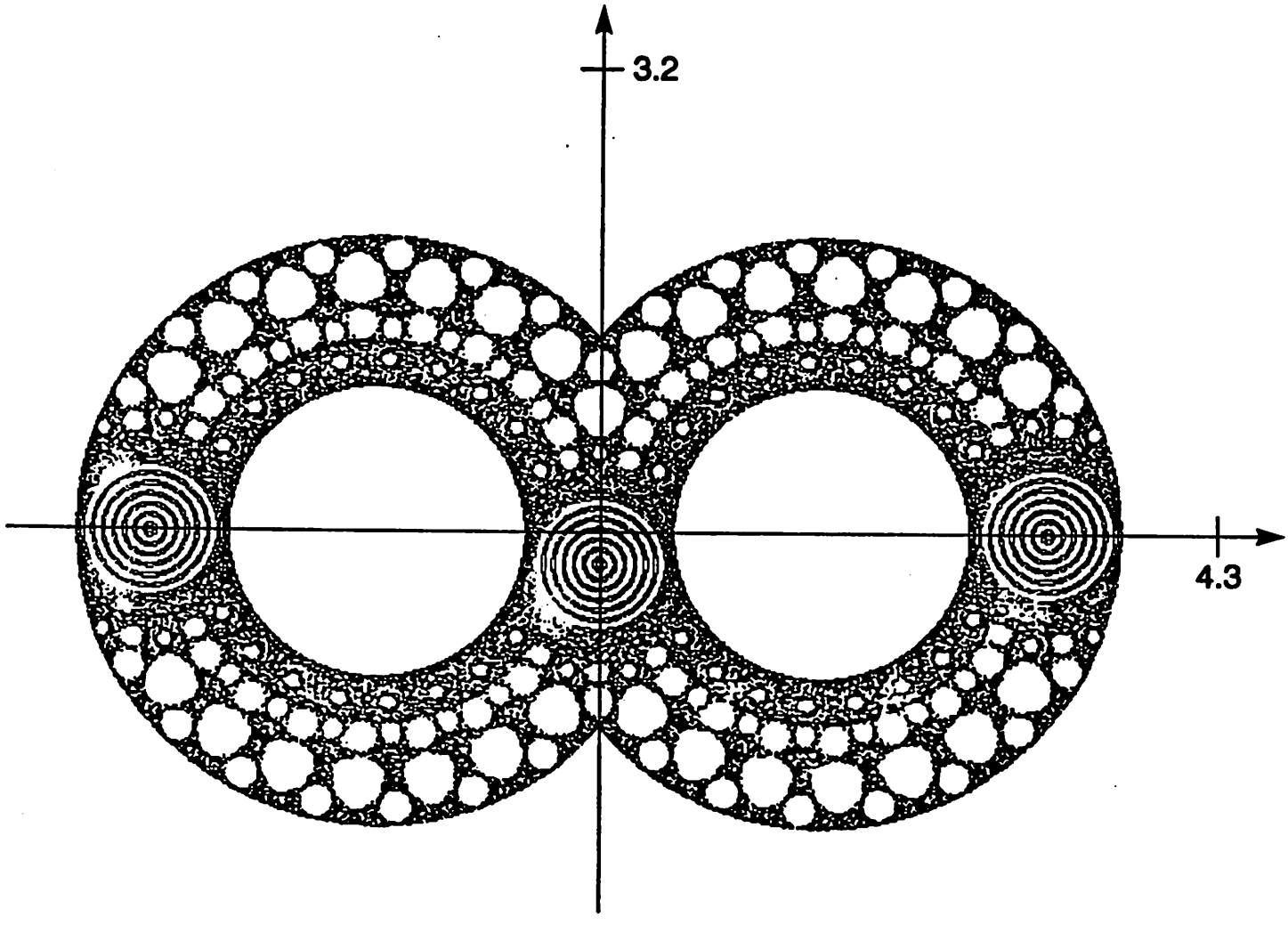

Fig. 11(g)

perturbation of circuit parameters. The second is the approximation of cantori, fractals which form barriers to the movement of a dynamical system. It is these barriers that may provide a mechanism for using limit cycles as a means of computing.

5.1 Breakup of elliptic regions and KAM circles under perturbation of circuit parameters

We now demonstrate the breakup of elliptic regions under small perturbations using the simple twist-and-flip map with $a = 1.7943$ and $\omega = \pi$. Figure 10(a) shows a region of the Poincaré phase plane of the simple twist-and-flip map around the fixed point (0.0,-3.6394). Before the perturbation we see a large elliptic region where every point lies on a crescent shaped curve and whose iterates make up a quasi-periodic orbit. Hence, for a sufficiently small neighborhood of the fixed point, the map, restricted to each crescent shaped curve, is conjugate (i.e., equivalent) [7] to an irrational rotation of the circle. After a small perturbation of the parameter a of 0.05 (see Fig. 10(b)), this elliptic region has broken up into two smaller elliptic regions, and the elliptic fixed point has become hyperbolic. This particular break up of an elliptic region into two smaller regions separated by a homoclinic tangle is fundamental to the design of a signal detector [14].

FIGURE 11(a) through (f)

A further illustration of the break-up of KAM circles can be seen in the following sequence of figures based on the twist-and-flip circuit having a square-pulse rotation function, with $r_0 = 3.0, n = 1000$, $a = 1.995$ and $\omega = \pi$. Beginning with Fig. 11(a) we see a series of 15 KAM circles on which the twist-and-flip acts like an irrational rotation of a circle. With a small change in the value of a from 1.995 to 1.99(Fig. 11(b)) we see the outermost circle break down into small elliptic and hyperbolic regions that have not been resolved clearly enough to recognize. At present the structure of the former outer ring simply appears to be a "random" set of points that make up the orbit starting from initial conditions (3.78,0.0) in the phase plane. When a is decreased to the value 1.9 (Fig. 11(c)), rings 13,14 also break up into a more distinct combination of elliptic regions. The empty holes represent elliptic

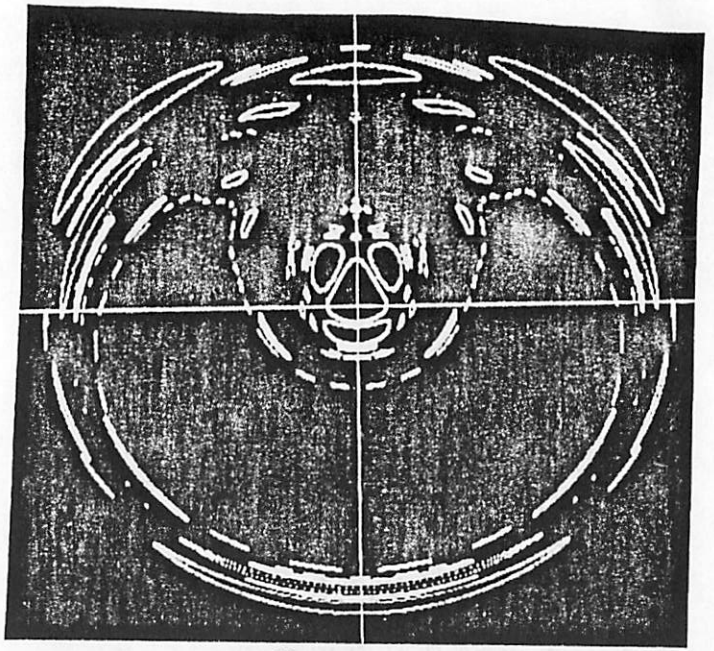

Fig 12 (a)

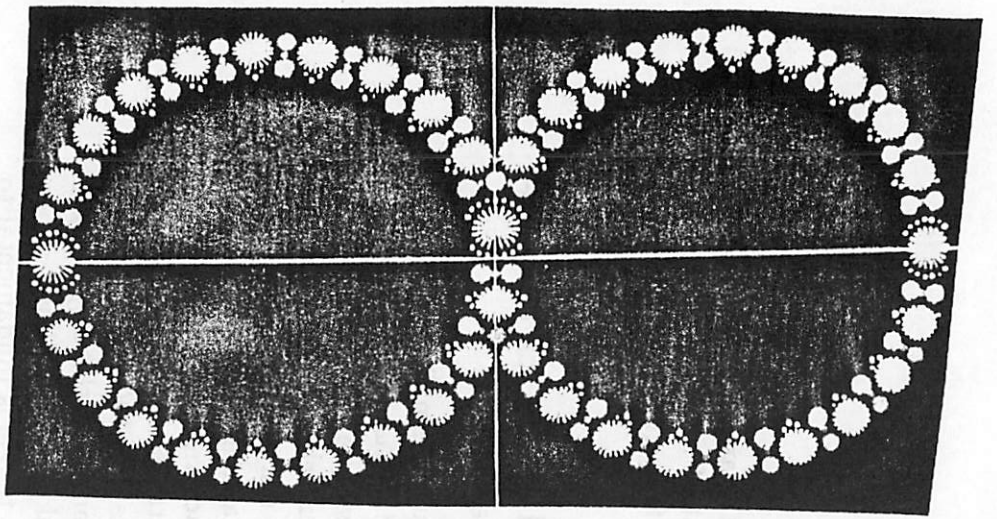

Fig 13 (a)

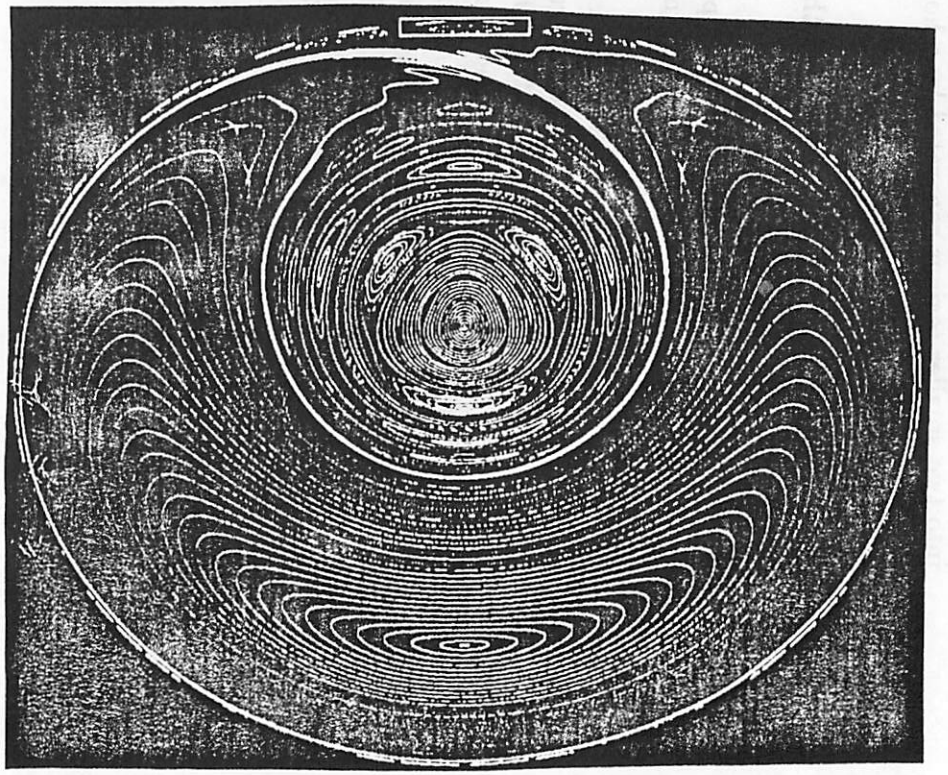

Fig 12 (c)

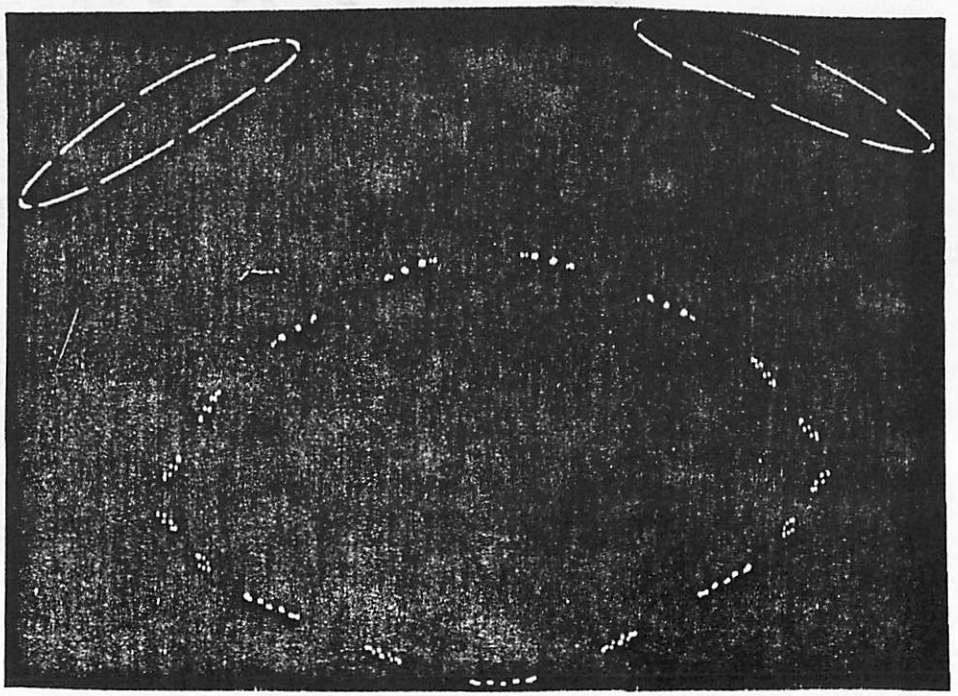

Fig 12 (d)

regions with island chains which we have not resolved. Decreasing a to 1.8 (Fig. 11(d)) we see the formation of a period-three region with island chains around it due to the breakdown of rings 10,11,12. Figs. 11(e) and 11(f) show the continuation of this process for $a = 1.7$ and $a = 1.6$ respectively. When $a = 1.5$ in Fig. 11(g), all of the original KAM circles are gone.

5.2 Approximation of cantori using the twist-and-flip map

Cantori are cantor sets known to exist in Hamiltonian systems and even in simple maps of the unit circle onto itself. They have been extensively studied by numerous researchers including Denjoy, Mather, Katok, Percival and others. The highly mathematical nature of this subject makes it impossible to discuss here except in the most heuristic terms. For those desiring to delve into this subject a starting point can be found in [7], section 6.4.1. The term "cantori" is not used in this reference but can be found in [15], and seems to be a term used by physicist's. It is not clear that the physicist and mathematicians are really discussing the same object but what is true is that the physicist concept of cantori is nevertheless a useful and important one and we illustrate it here using the twist-and-flip map.

The interest in cantori and fractal-like sets of elliptic regions is due to the manner in which they form a barrier to transport in Hamiltonian systems [15]. Rather than explain what is meant by the physicist, we will illustrate how fractal-like elliptic regions are a barrier to movement.

In Fig. 12(a) is shown 16 sets of elliptic regions for the simple twist-and-flip map FT, where ($a = 1.0$, $\omega = 2\pi$), obtained by selecting an initial condition and iterating FT until a set of closed curves has been formed. For example, the regions which look like the two eyes and a mouth are all formed from the same initial condition $(0.0, -0.76)$. The interior of these curves forms a set of regions, and for each set there is a k for which that set is invariant for $(\mathrm{FT})^k$. The union of all of these regions is therefore invariant under FT. The symmetry of this set of elliptic regions is due to property 6 of section 3.

If we start outside of all of these regions at the point (0.0, 9.0) and iterate 200,000 times we get Fig. 12(b). Note that this orbit contains a number of holes of various shapes. They match exactly the elliptic regions seen in

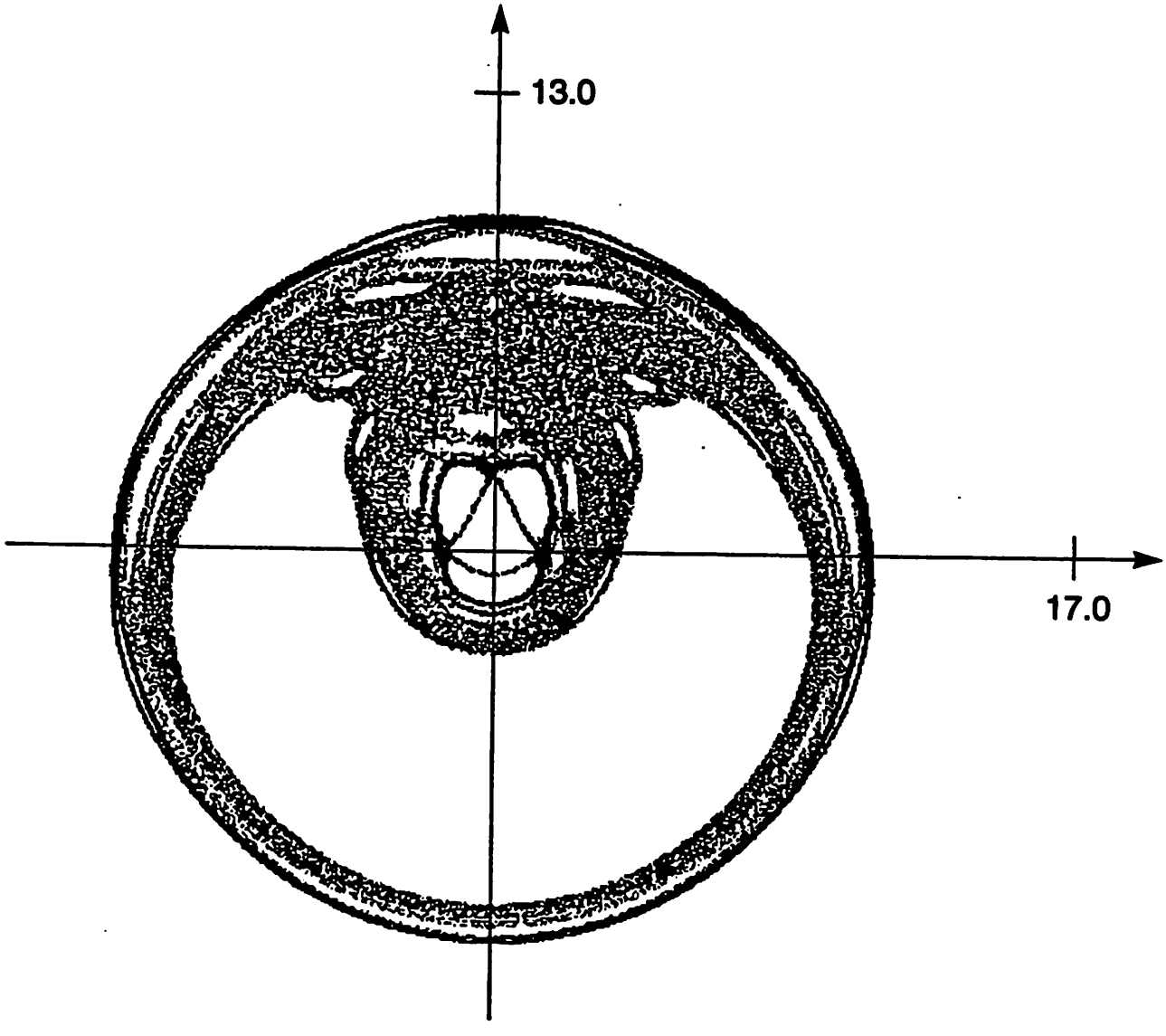

Fig. 12(b)

Fig. 12(a). Thus, from the looks of this figure, it appears that the set of elliptic regions in Fig. 12 form some sort of barrier to the orbit of this point. Since the elliptic regions are invariant, if we start outside of one we can never enter it. But there are gaps between these regions, i.e., they do not form a solid barrier. We can ask: why doesn't the orbit of our initial point pass through one of these gaps? One reason is there are still more, smaller elliptic regions between these gaps that are not shown in Fig. 12(a). These additional regions are of smaller and smaller size and collectively make it very improbable that an orbit will pass through them. Hence these regions that are collectively fractal-like in that they exist on all scales may be said to form a barrier to "transport".

The elliptic regions, however numerous, cannot touch one another, and hence must have a boundary. This boundary can be a Cantor set and is, in any case, a fractal. When it forms an invariant Cantor set, it is called a cantori. The 'tori' part of this word comes from the word 'torus', which is what the elliptic regions look like for three-dimensional twist-and-flip maps. The cantori are also barriers to the orbits of FT. The elliptic regions in Fig. 12(a) are just fractal-like. However, Fig. 12(c) contains an approximation to a cantori. The map used is the simple twist-and-flip map with $a = .3214$, $\omega = \pi$. The approximate cantori is the outermost set of elliptic regions in yellow. They can best be seen at the top of the figure but they completely encircle the figure. Also shown are a set of outer most blue elliptic regions that encircle the approximation of the cantori. Also in yellow is an unstable manifold for a hyperbolic fixed point at (0.0, 3.234). It appears trapped inside the shell of elliptic regions. By property 7 the stable manifold (not shown) is the reflection of the unstable manifold about the vertical axis which runs directly through the center of the figure (the vertical axis is also not shown). If the stable manifold were shown we would see a set of homoclinic tangles near the top of the figure where the unstable manifold begins to oscillate. The yellow unstable manifold also has an interior boundary seen as a set of blue and red elliptic regions where cantori might also be found. The interior blue region is broken up into more elliptic regions and will have island chains which are not shown. The part of the figure inside the white rectangular box is enlarged in Fig. 12(d).

The approximation is obtained by starting with a KAM circle for $a = 0.0$ and slowly varying a and keeping track of the breakup of the original circle into ever smaller elliptic regions as a is increased. With patience, this process

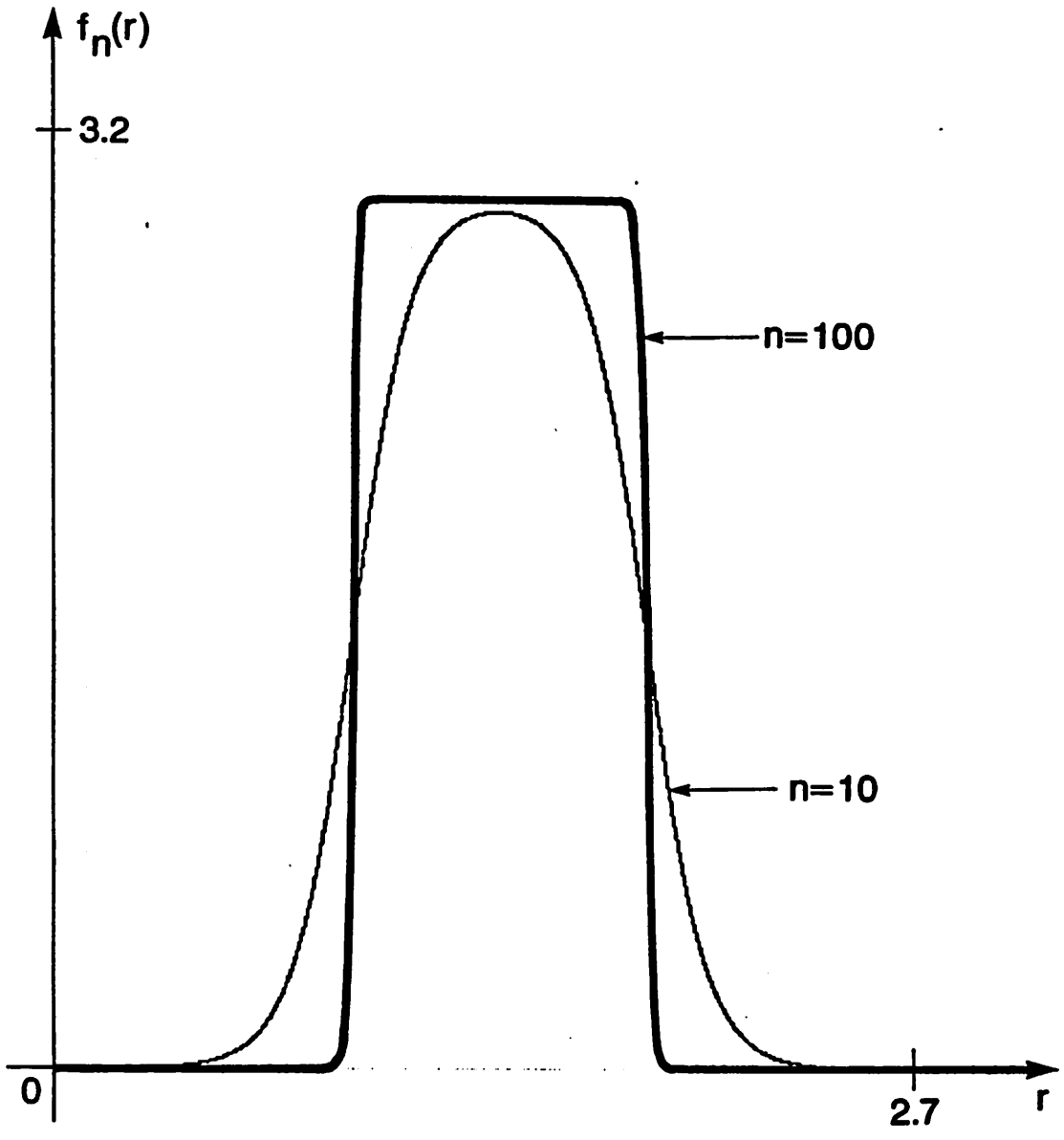

Fig. 13(b)

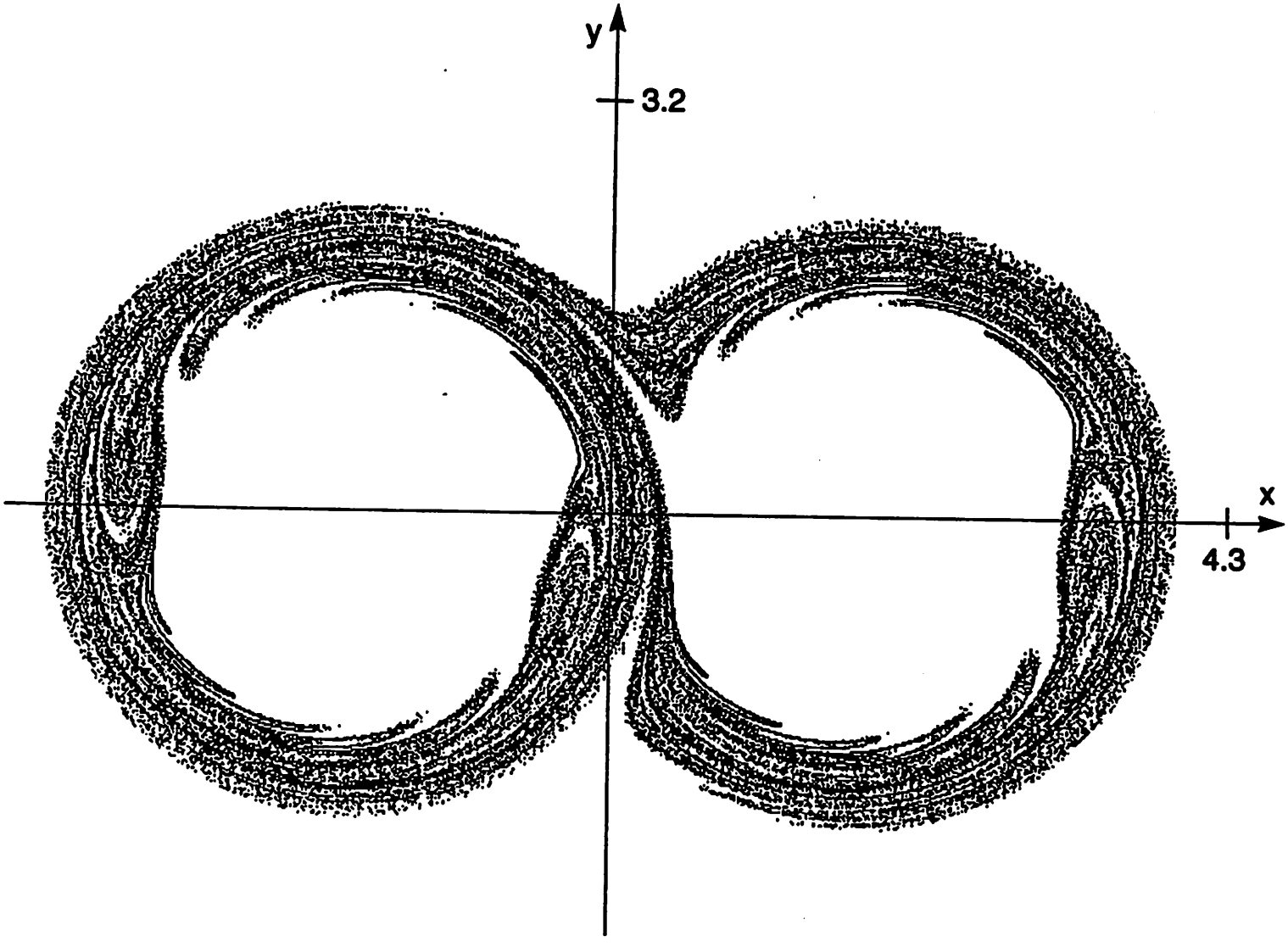

Fig. 13(c)

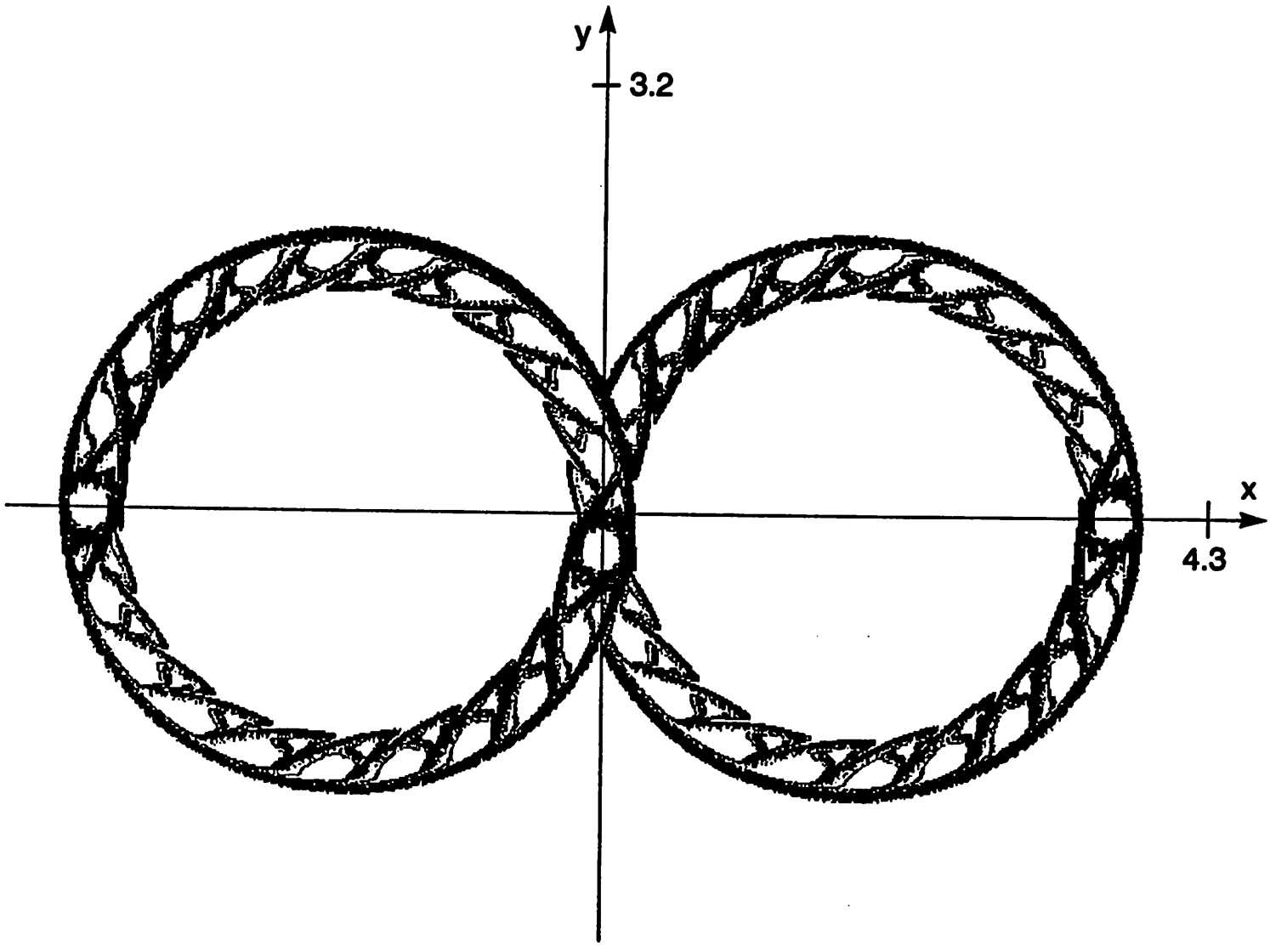

Fig. 13(d)

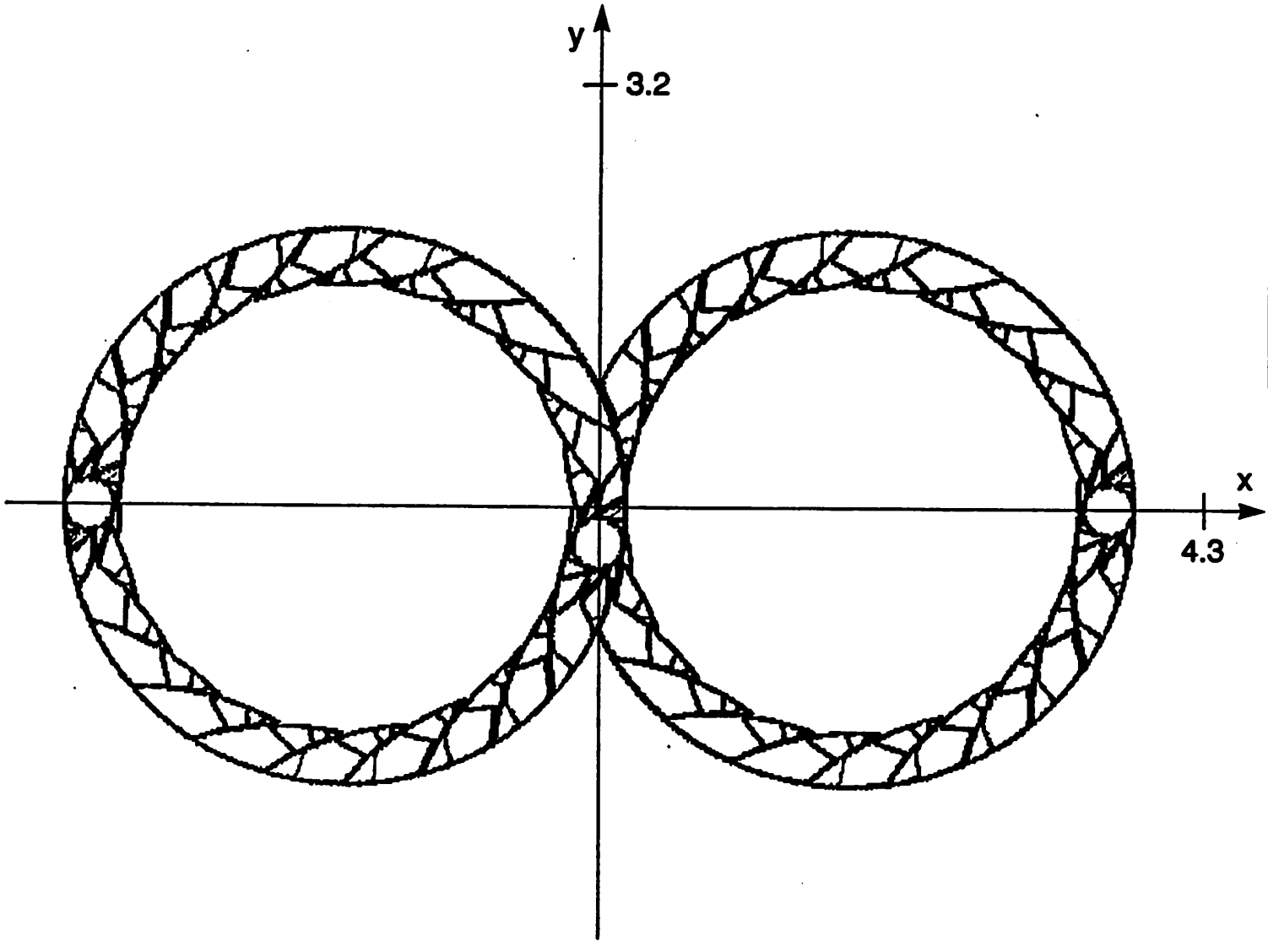

Fig. 13(e)

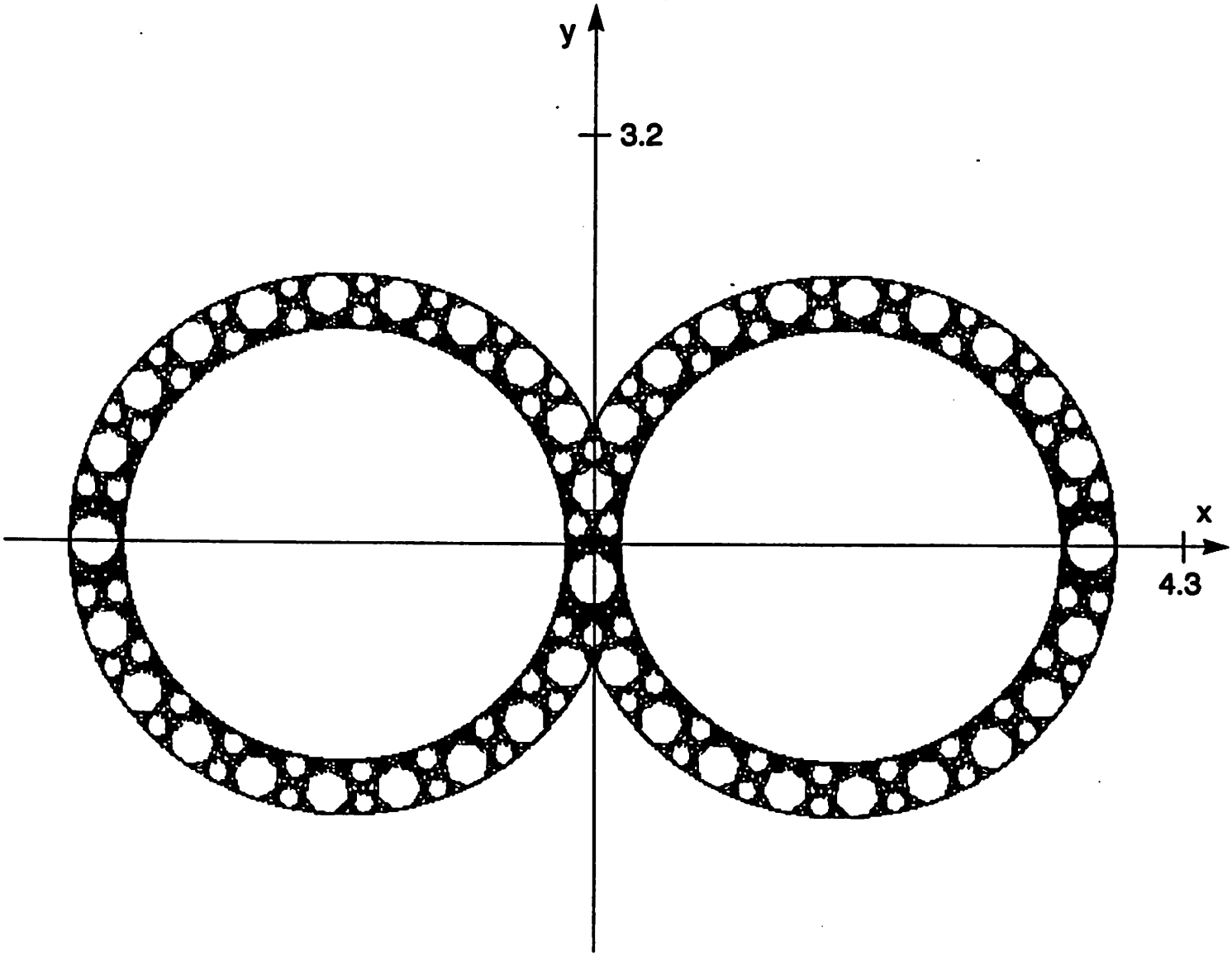

Fig. 13(f)

could be continued until the regions appeared to be made up of dust sized particles.

6 Mathematical Characterization of the Fractals Associated with the Twist-and-Flip Circuit

In this section we want to illustrate the relationship of the fractal boundary of the elliptic regions found the Poincaré map of subsection 4.3 and a sequence of stable and unstable manifolds that produce homoclinic tangles.

The significance of this is that if we remove the union of all of these open sets from the two annuli, what is left is a closed set. In fact, since it is a Cantor set, it is a fractal. As demonstrated by the figures in Sec.4, the twist-and-flip circuit generates such fractals easily. We will now illustrate how this fractal set is the limit of a sequence of unstable manifolds of twist-and-flip maps. We will do this by constructing a sequence of rotation functions for the twist-and-flip maps that converges pointwise to the square-pulse rotation function shown in Fig. 8(a).

The sequence of rotation functions is given by the following formula:

$$f_n(r) = 0.5\, r_0\, (h_n(r-1) - h_n(r-2))$$

where

$$h_n(r) = (\exp(nr) - 1)/(\exp(nr) + 1)$$

We note that the pointwise limit of $h_n(r)$ is $\mathrm{sgn}(r)$, except at two points, as $n \to \infty$ so that the limit of $f_n(r)$ is

$$0.5\, r_0(\mathrm{sgn}(r-1) - \mathrm{sgn}(r-2))$$

which is a square-pulse of magnitude r_0 for $1 \leq r \leq 2$ and 0.0 elsewhere.

FIGURE 13(b) through (f)

Figure. 13(b) is the graph of $f_n(r)$ for $n = 10.0, 100.0, 1000.0$. Also shown is the limit of the f_n, the square-pulse function.

We want to see what happens to the unstable manifold W_p^u for this twist-and-flip map as $n \to \infty$.

Figures 13(c)- 13(f) show the unstable manifold of FT as n ranges over the values $10, 100, 300$ and 2000. In each case $a = 1.8$, $\omega = \pi$. To generate an image of the unstable manifold we use a line segment tangent to the unstable manifold at the fixed point of length 0.01 divided into 5000 steps and iterated 55 times. In each figure caption is listed the location of the fixed point and the slope of the unstable manifold at that fixed point.

As can be seen in the sequence of figures, the unstable manifold is becoming confined to the narrow annulus of Fig. 13(a). We know from Sec.3 that the stable manifold and unstable manifold are symmetric about the vertical axis, as is the union of the two annuli and hence they are "converging" in some sense to the region not occupied by the union of the elliptic regions shown in Fig. 13(a). In fact the union of the elliptic regions and the union of the unstable and stable manifolds share a common boundary. As $n \to \infty$, the elliptic regions continue to grow in total area, and thus the area left over for the stable and unstable manifolds becomes smaller. In the limit, we conjecture that the union of the stable and unstable manifolds is "absorbed" into the boundary of the union of the elliptic regions. This conjecture seems to suggest that the fractal boundary of the union of the elliptic regions is in some sense an analogue of the union of the stable and unstable manifolds. We note that in the limit, the elliptic regions appear to converge to some maximum size, but that in the limit, the unstable manifold vanishes. This conjecture is further reinforced by the fact that the hyperbolic fixed point approaches the point (0.0,0.87177), and the slope of the unstable manifold approaches the slope $-a/y$. Thus near the fixed point, the stable and unstable manifolds blend into the outer rings of the two annuli. But more interesting still is that the point (0.0,0.87177) is not a fixed point for the twist-and-flip map with the square-pulse rotation function.

7 Concluding Remarks

We have tried to show, in this paper, the broad array of fractal images that can be produced by the twist-and-flip circuit. Although the real physical realization of a circuit is by necessity not a lossless device, the dynamics of this physical realization are nevertheless shaped by the fractal dynamics that

are found in the twist-and-flip map which is lossless. It can be shown that when a damping factor is added to the twist-and-flip map [6], Sec. 12.0 it does not remove the fractals that already exist there. These fractals continue to influence the circuit through transients of a very long duration and through the formation of fractal attractors any of which can be of the form we have illustrated. In fact a very large damping factor is needed to eliminate chaos in these circuits when it exists [6].

What is particularly important is that by the variation of the parameters of the twist-and-flip circuit and the use of a damping parameter, it is possible to vary the fractal images the circuit can produce and due to the kaleidoscopic nature of these images it may be possible to encode information in these fractals. Simply put, the twist-and-flip circuit provides the possibility of developing a new type of computer that utilizes the multitude of fractal phenomena found in the twist-and-flip map as a computing device.

In another direction, the fact that the complexity present in this circuit is unlimited in variety and scope, and the fact that an extensive theoretical foundation exist for the twist-and-flip map makes it a very desirable and interesting object for modeling and experimentation. What seems certain is that the array of fractals that can now be shown to arise in circuits due to the twist-and-flip circuit suggests that the study of circuits may take on equal importance as the use of software tools in the field of modeling, simulation and scientific experimentation.

Pedagogically, the twist-and-flip circuit provides the simplest two-dimensional model of chaos that is an accurate paradigm for all two-dimensional chaos that arises from systems described by periodically forced ordinary differential equations.

References

[1] T. Matsumoto, "A Chaotic Attractor from Chua's Circuit", *IEEE Transactions on Circuits and Systems*, Vol. **31**, no.12, pp.1055-1058, 1984.

[2] "The Genesis of Chua's Circuit", *Archiv fur Elektronik und Ubertragungstechnik* (International Journal of Electronics and Communications), to appear in 1992.

[3] R. N. Madan (Guest Editor), Special Issue on "Chua's Circuit: A Paradigm for Chaos", *Journal of Circuits, Systems and Computers*, March 1993.

[4] P. Kennedy, "Robust Op Amp realization of Chua's circuit", *Frequency*, Vol. 46, no.3-4, March-April, 1992.

[5] R. Brown and L. Chua, "Horseshoes in the twist-and-flip map", *International Journal of Bifurcation and Chaos*, vol.1 no.1, pp.235-252, 1991.

[6] R. Brown and L. Chua, "Generalizing the twist-and-flip paradigm", *International Journal of Bifurcation and Chaos*, vol.1 no.2, pp.385-416, 1991.

[7] D.K.Arrowsmith and C. M. Place, *An Introduction to Dynamical Systems.* Cambridge University Press, 1990

[8] L.O.Chua, *Introduction to Nonlinear Network Theory.* McGraw-Hill, 1969

[9] L.O.Chua, C.A.Desoer and E.S. Kuh *Linear and Nonlinear Circuits.* McGraw-Hill, 1985

[10] T.S.Parker and L.O.Chua, *Practical Numerical Algorithms for Chaotic Systems.* Springer-Verlag, 1989

[11] R.L.Devaney, *An Introduction to Chaotic Dynamical Systems.* Addison Wesley, 1989.

[12] M. Henon "Numerical Study of Quadratic Area-Preserving Mappings". *Quarterly of Applied Mathematics*, vol XXVII, No, 3 1969

[13] R. Brown and L. Chua, "Generalizing the twist-and-flip paradigm II", *International Journal of Bifurcation and Chaos*, vol.1 no.4, 1991.

[14] R. Brown, L. Chua, and B. Popp "Is Sensitive Dependence on Initial Conditions Natures Sensory Device?" *International Journal of Bifurcation and Chaos*, vol.1 no.4, 1991.

[15] R. S. Mackay, J.D. Meiss and I.C. Percival, "Transport in Hamiltonian Systems", *Physica D*, 13, pp.55-81,(1984)

List of Figure Captions

Fig. 1

(a) The twist-and-flip circuit containing a gyrator characterized by a non-linear gyration conductance function $g(v_1, v_2)$.

(b) The voltage source in (a) is a square-wave with amplitude a and angular frequency ω.

Fig. 2

(a) The integral curves for the twist-and-flip circuit during the half period where $s(t) = a$.

(b) The integral curves for the twist-and-flip circuit during the half period where $s(t) = -a$.

(c) Combined integral curves for the twist-and-flip circuit over a full period.

Fig. 3

(a) Fifty cycles of a phase-plane trajectory for the simple (with $f(r) = r$) twist-and-flip circuit from a single initial condition, (0,0 8.0). $a = 1.0$, $\omega = \pi$.

(b) Fifty iterations of a phase-plane orbit for the Poincaré map, FT, of the simple twist-and-flip circuit from a single initial condition, (0,0 8.0). These fifty points correspond to strobing the continuous trajectory from (a) once every half period ($P/2 = \pi/\omega$).

Fig. 4

(a) A single period of the phase plane orbit for the simple twist-and-flip circuit from a single initial condition 1, at $t = 0$.

(b) The orbit from (a) drawn with the two relevant circles of radius r_1 and r_2, and the reflection of the left circle centered at ($-a$, 0.0) into the right circle centered at (a, 0.0).

(c) The Poincaré map FT(1) can be obtained by first reflecting the point A into B , and then locating C and reflecting it to obtain point 2.

Fig. 5

(a) The simple twist-and-flip map, FT, 4000 times starting from the point (5.4, 0). The iterates of this point circulate around the three crescent shaped curves in a sequential rather than random manner. $a = 1.0,\ \omega = \pi$.

(b) A graphical procedure for locating a fixed point on the vertical axis. The fixed point is located at $(0.0, 1.955)$.

Fig. 6

(a) Elliptic and hyperbolic regions of a simple twist-and-flip map $a = 1.0$, $\omega = \pi$. The center of this figure is approximately located at (0.0, 6.2031) and is an elliptic periodic point of period 2. (0.0, 1.95512)

(b) An extensive homoclinic tangle in green from the hyperbolic fixed point $(0.0, 1.955)$ for the same simple twist-and-flip map as in (a).

(c) An enlargement of the small yellow region in (b) showing that it is composed of a set of island chains.

Fig. 7

(a) The elliptic and hyperbolic regions for the twist-and-flip map having the gyration conductance function $f(r) = 1/r$. $a = 0.2$, $\omega = \pi$. Period-9 hyperbolic point is at (0.0, 0.134).

(b) The graph of the gyration conductance function $f(r) = 1/r$.

(c) The elliptic and hyperbolic regions for the twist-and-flip map having the gyration conductance function $f(r) = (r + \log(r))/r^2$. $a = 0.2$, $\omega = \pi$. A hyperbolic fixed point is at (0.0, 0.318).

(d) The graph of the gyration conductance function $f(r) = (r+\log(r))/r^2$.

Fig. 8

(a) The graph of the gyration conductance function described by the square-pulse $f(r) = .5r_0(\mathrm{sgn}(r-1) - \mathrm{sgn}(r-2))$.

(b) The annulus on which all dynamics are generated for the square-pulse gyration conductance function.

(c) The union of the two annuli on which all dynamics occurs for the square-pulse gyration conductance function.

(d) A set of intervals surrounding the elliptic periodic points on the vertical axis are removed to form a Cantor set. The Cantor set is formed by deleting the entire interval around the periodic point and leaving the end points of the interval.

(e) 100,000 iterates of the point (0.0, -0.4486) showing the outline of a fractal image.

Fig. 9

(a) The outline of the fractal image for a three-region stair-case gyration conductance function with $a = 5.0$ and $\omega = \pi$.

(b) The outline of the fractal image for a two-region stair-case gyration conductance function with $a = 1.0$ and $\pi = \omega$.

(c) The outline of the fractal image for a three-region stair-case gyration conductance function with $a = 1.0$ and $\omega = \pi$.

Fig. 10

(a) The large elliptic region (yellow) around the point (0.0, -3.6394), $a = 1.7943$, $\omega = \pi$.

(b) A bifurcation for a large elliptic region around the point (0.0, -3.6394), into two elliptic regions (red) surrounded by an unstable manifold (yellow). $a = 1.7943$, $\omega = \pi$.

Fig. 11

(a) Phase-plane orbits for the twist-and-flip map showing 15 concentric KAM circles centered around a period-two point, (a, 0.0), of FT. $a = 1.995$, $\omega = \pi$.

(b) Phase-plane orbits for the twist-and-flip map showing the breakdown of the outermost circle, the fifteenth circle counting from inside out, into smaller regions and homoclinic tangles (the homoclinic tangles are not shown). $a = 1.99$, $\omega = \pi$.

(c) Phase-plane orbits for the twist-and-flip map showing the breakdown of circles 13,14,15 into smaller regions and tangles. $a = 1.9$, $\omega = \pi$

(d) Phase-plane orbits for the twist-and-flip map showing the breakdown of circles 10,11,12 into smaller regions and tangles. $a = 1.8$, $\omega = \pi$

(e) Phase-plane orbits for the twist-and-flip map showing the breakdown of circles 7 through 15 into smaller regions and tangles. $a = 1.7$, $\omega = \pi$

(f) Phase-plane orbits for the twist-and-flip map showing the breakdown of circles 4 through 15 into smaller regions and tangles. $a = 1.6$, $\omega = \pi$

(g) Phase-plane orbits for the twist-and-flip map showing the breakdown of all KAM circles 1 through 15 into smaller regions and tangles. $a = 1.5$, $\omega = \pi$

Fig. 12

(a) Phase-plane orbits for the simple twist-and-flip map showing numerous elliptic regions of varying sizes. $a = 1.0$, $\omega = 2\pi$.

(b) 200,000 iterates of the simple twist-and-flip map starting from (0.0, 9.0). $a = 1.0$, $\omega = 2\pi$.

(c) An approximation to a cantori for the simple twist-and-flip map showing numerous small elliptic regions surrounding an unstable manifold at the hyperbolic fixed point (0.0, 3.234). $a = .3241$, $\omega = \pi$.

(d) An enlargement of the area inside the white rectangular box in (c).

Fig. 13

(a) Small circular phase plane orbits for the piece-wise linear twist-and-flip map $a = 1.8$, $\omega = \pi$, $f(r) = .5r_0(\mathrm{sgn}(r-1) - \mathrm{sgn}(r-2))$. After removal of all such orbits only a Cantor set remains.

(b) The graph of the gyration conductance functions $f_n(r) = .5r_0(h_n(r-1) - h_n(r-2))$, for $n = 10$, and $n = 100$.

(c) The unstable manifold for the twist-and-flip map for $a = 1.8$, $\omega = \pi$, $f_n(r) = .5r_0(h_n(r-1) - h_n(r-2))$, $n = 10$. A hyperbolic fixed point is located at (0.0, 1.013).

(d) The unstable manifold for the twist-and-flip map for $a = 1.8$, $\omega = \pi$, $f_n(r) = .5r_0(h_n(r-1) - h_n(r-2))$, $n = 100$. A hyperbolic fixed point is located at (0.0, 0.8904).

(e) The unstable manifold for the twist-and-flip map for $a = 1.8$, $\omega = \pi$, $f_n(r) = .5r_0(h_n(r-1) - h_n(r-2))$, $n = 300$. A hyperbolic fixed point is located at (0.0, 0.87814).

(f) The unstable manifold for the twist-and-flip map for $a = 1.8$, $\omega = \pi$, $f_n(r) = .5r_0(h_n(r-1) - h_n(r-2))$, $n = 2000$. A hyperbolic fixed point is located at (0.0, 0.87275).